

REPORT DOCUMENTATION PAGE			Form Approved OMB NO. 0704-0188		
<p>The public reporting burden for this collection of information is estimated to average 1 hour per response, including the time for reviewing instructions, searching existing data sources, gathering and maintaining the data needed, and completing and reviewing the collection of information. Send comments regarding this burden estimate or any other aspect of this collection of information, including suggestions for reducing this burden, to Washington Headquarters Services, Directorate for Information Operations and Reports, 1215 Jefferson Davis Highway, Suite 1204, Arlington VA, 22202-4302. Respondents should be aware that notwithstanding any other provision of law, no person shall be subject to any penalty for failing to comply with a collection of information if it does not display a currently valid OMB control number.</p> <p>PLEASE DO NOT RETURN YOUR FORM TO THE ABOVE ADDRESS.</p>					
1. REPORT DATE (DD-MM-YYYY) 11-05-2011		2. REPORT TYPE Final Report		3. DATES COVERED (From - To) 13-Oct-2010 - 11-Apr-2011	
4. TITLE AND SUBTITLE Compact & Ultra-High Resolution Terahertz Spectroscopic/Fingerprint System			5a. CONTRACT NUMBER		
			5b. GRANT NUMBER W911NF-11-C-0005		
			5c. PROGRAM ELEMENT NUMBER 665502		
6. AUTHORS Shi, Wei; Petersen, Eliot; Chavez-Pirson, Arturo			5d. PROJECT NUMBER		
			5e. TASK NUMBER		
			5f. WORK UNIT NUMBER		
7. PERFORMING ORGANIZATION NAMES AND ADDRESSES NP Photonics, Inc. UA Science & Tech Park 9030 S. Rita Road, Suite 120 Tucson, AZ 85747 -9108			8. PERFORMING ORGANIZATION REPORT NUMBER		
9. SPONSORING/MONITORING AGENCY NAME(S) AND ADDRESS(ES) U.S. Army Research Office P.O. Box 12211 Research Triangle Park, NC 27709-2211			10. SPONSOR/MONITOR'S ACRONYM(S) ARO		
			11. SPONSOR/MONITOR'S REPORT NUMBER(S) 58680-EL-ST1.1		
12. DISTRIBUTION AVAILABILITY STATEMENT Approved for Public Release; Distribution Unlimited					
13. SUPPLEMENTARY NOTES The views, opinions and/or findings contained in this report are those of the author(s) and should not be construed as an official Department of the Army position, policy or decision, unless so designated by other documentation.					
14. ABSTRACT Report developed under topic #A10A-T013, contract W911NF-11-C-005. In Phase I, NP Photonics has successfully demonstrated the feasibility to implement the proposed fiber-based, compact, tunable, THz spectroscopic/fingerprinting system. We have achieved 0.212 mJ fiber laser pulses with transform-limited linewidth, bonded QPM-GaP crystals and the proposed THz crystal fiber converters for high power parametric THz source, THz waveguide modeling for high efficiency and high power THz generation, THz power 0.339 mW based					
15. SUBJECT TERMS Terahertz frequency, waveguide devices, fiber lasers/amplifiers, THz up-conversion, THz spectroscopic/fingerprinting system, chemical and biological agent, explosives detection					
16. SECURITY CLASSIFICATION OF:		17. LIMITATION OF ABSTRACT		15. NUMBER OF PAGES	19a. NAME OF RESPONSIBLE PERSON
a. REPORT UU	b. ABSTRACT UU	c. THIS PAGE UU	UU		Wei Shi
					19b. TELEPHONE NUMBER 520-799-7413

Report Title

Compact & Ultra-High Resolution Terahertz Spectroscopic/Fingerprint System

ABSTRACT

Report developed under topic #A10A-T013, contract W911NF-11-C-005. In Phase I, NP Photonics has successfully demonstrated the feasibility to implement the proposed fiber-based, compact, tunable, THz spectroscopic/fingerprinting system. We have achieved 0.212 mJ fiber laser pulses with transform-limited linewidth, bonded QPM-GaP crystals and the proposed THz crystal fiber converters for high power parametric THz source, THz waveguide modeling for high efficiency and high power THz generation, THz power 0.339 mW based on an external cavity enhancement. We have successfully demonstrated room temperature THz detection based-on THz upconversion by using the QPM-GaP crystal that will be used to develop the fiber-based high-resolution THz spectrometer in Phase II.

List of papers submitted or published that acknowledge ARO support during this reporting period. List the papers, including journal references, in the following categories:

(a) Papers published in peer-reviewed journals (N/A for none)

Number of Papers published in peer-reviewed journals: 0.00

(b) Papers published in non-peer-reviewed journals or in conference proceedings (N/A for none)

Number of Papers published in non peer-reviewed journals: 0.00

(c) Presentations

Number of Presentations: 0.00

Non Peer-Reviewed Conference Proceeding publications (other than abstracts):

Number of Non Peer-Reviewed Conference Proceeding publications (other than abstracts): 0

Peer-Reviewed Conference Proceeding publications (other than abstracts):

Number of Peer-Reviewed Conference Proceeding publications (other than abstracts): 0

(d) Manuscripts

Number of Manuscripts: 0.00

Patents Submitted

Patents Awarded

Awards

Graduate Students

<u>NAME</u>	<u>PERCENT SUPPORTED</u>
FTE Equivalent:	
Total Number:	

Names of Post Doctorates

<u>NAME</u>	<u>PERCENT SUPPORTED</u>
FTE Equivalent:	
Total Number:	

Names of Faculty Supported

<u>NAME</u>	<u>PERCENT SUPPORTED</u>
FTE Equivalent:	
Total Number:	

Names of Under Graduate students supported

<u>NAME</u>	<u>PERCENT SUPPORTED</u>
FTE Equivalent:	
Total Number:	

Student Metrics

This section only applies to graduating undergraduates supported by this agreement in this reporting period

The number of undergraduates funded by this agreement who graduated during this period: 0.00

The number of undergraduates funded by this agreement who graduated during this period with a degree in science, mathematics, engineering, or technology fields:..... 0.00

The number of undergraduates funded by your agreement who graduated during this period and will continue to pursue a graduate or Ph.D. degree in science, mathematics, engineering, or technology fields:..... 0.00

Number of graduating undergraduates who achieved a 3.5 GPA to 4.0 (4.0 max scale):..... 0.00

Number of graduating undergraduates funded by a DoD funded Center of Excellence grant for Education, Research and Engineering:..... 0.00

The number of undergraduates funded by your agreement who graduated during this period and intend to work for the Department of Defense 0.00

The number of undergraduates funded by your agreement who graduated during this period and will receive scholarships or fellowships for further studies in science, mathematics, engineering or technology fields: 0.00

Names of Personnel receiving masters degrees

<u>NAME</u>
Total Number:

Names of personnel receiving PhDs

NAME

Total Number:

Names of other research staff

NAME

PERCENT SUPPORTED

Wei Shi	0.10	No
Eliot Petersen	0.20	No
Dan Nguyen	0.20	No
Jie Zong	0.10	No
Sterling Fritz	0.10	No
FTE Equivalent:	0.70	
Total Number:	5	

Sub Contractors (DD882)

Inventions (DD882)

Scientific Progress

See Attachment

Technology Transfer

REPORT DOCUMENTATION PAGE

*Form Approved
OMB No. 0704-0188*

The public reporting burden for this collection of information is estimated to average 1 hour per response, including the time for reviewing instructions, searching existing data sources, gathering and maintaining the data needed, and completing and reviewing the collection of information. Send comments regarding this burden estimate or any other aspect of this collection of information, including suggestions for reducing the burden, to Department of Defense, Washington Headquarters Services, Directorate for Information Operations and Reports (0704-0188), 1215 Jefferson Davis Highway, Suite 1204, Arlington, VA 22202-4302. Respondents should be aware that notwithstanding any other provision of law, no person shall be subject to any penalty for failing to comply with a collection of information if it does not display a currently valid OMB control number.

PLEASE DO NOT RETURN YOUR FORM TO THE ABOVE ADDRESS.

1. REPORT DATE (DD-MM-YYYY) 05/11/2011		2. REPORT TYPE Final Technical Report		3. DATES COVERED (From - To) 10/13/2010 - 04/11/2011	
4. TITLE AND SUBTITLE Compact & Ultra-High Resolution Terahertz Spectroscopic/Fingerprint System				5a. CONTRACT NUMBER W911NF-11-C-0005	
				5b. GRANT NUMBER	
				5c. PROGRAM ELEMENT NUMBER	
6. AUTHOR(S) Shi, Wei Petersen, Eliot Chavez-Pirson, Arturo				5d. PROJECT NUMBER	
				5e. TASK NUMBER	
				5f. WORK UNIT NUMBER	
7. PERFORMING ORGANIZATION NAME(S) AND ADDRESS(ES) NP PHOTONICS, INC 9030 S. RITA RD STE 120 TUCSON AZ 85747-9102				8. PERFORMING ORGANIZATION REPORT NUMBER	
9. SPONSORING/MONITORING AGENCY NAME(S) AND ADDRESS(ES) US ARMY RDECOM ACQ CTR - W911NF 4300 S. MIAMI BLVD DURHAM NC 27703				10. SPONSOR/MONITOR'S ACRONYM(S)	
				11. SPONSOR/MONITOR'S REPORT NUMBER(S)	
12. DISTRIBUTION/AVAILABILITY STATEMENT Approve for Public Release; Distribution Unlimited					
13. SUPPLEMENTARY NOTES					
14. ABSTRACT Report developed under topic #A10A-T013, contract W911NF-11-C-005. In Phase I, NP Photonics has successfully demonstrated the feasibility to implement the proposed fiber-based, compact, tunable, THz spectroscopic/fingerprinting system. We have achieved 0.212 mJ fiber laser pulses with transform-limited linewidth, bonded QPM-GaP crystals and the proposed THz crystal fiber converters for high power parametric THz source, THz waveguide modeling for high efficiency and high power THz generation, THz power 0.339 mW based on an external cavity enhancement. We have successfully demonstrated room temperature THz detection based-on THz upconversion by using the QPM-GaP crystal that will be used to develop the fiber-based high-resolution THz spectrometer in Phase II.					
15. SUBJECT TERMS STTR Report; Terahertz frequency, waveguide devices, fiber lasers/amplifiers, THz up-conversion, THz spectroscopic/fingerprinting system, chemical and biological agent, explosives detection					
16. SECURITY CLASSIFICATION OF:			17. LIMITATION OF ABSTRACT SAR	18. NUMBER OF PAGES 27	19a. NAME OF RESPONSIBLE PERSON Leroy R. Hardy, Jr.
a. REPORT U	b. ABSTRACT U	c. THIS PAGE U			19b. TELEPHONE NUMBER (Include area code) 919-549-4237

Final Report

(10/13/2010-04/11/2011)

1.0 INTRODUCTION

In Phase I, NP Photonics has successfully demonstrated the feasibility to implement the proposed fiber-based, compact, tunable, THz spectroscopic/fingerprinting system, by achieving the progress as following:

- (1) The pulse energy of NP pulsed fiber lasers with transform-limited linewidth have been scaled up to 0.212 mJ, which corresponds to a peak power of 2.12 kW by using the new developed NP single-mode PM large core fiber 30/250. This pulse energy is the highest fiber-based pulse energy for the longer pulses (> 100 ns) with transform-limited linewidth.**
- (2) Achieved the bonded QPM-GaP crystals and the proposed THz crystal fiber converter for high power parametric THz source.**
- (3) Achieved the optimized coherence length for GaP crystal by using a GaP wedge, and demonstrated a new approach to verify the THz wavelength by using the GaP wedge.**
- (4) THz waveguide modeling has been developed for high efficiency and high power THz generation In Phase I by the UD team, which can be used for the design to fabricate the THz waveguide nonlinear crystal (or THz waveguide crystal converter) in NP Photonics, in order to achieve the high efficiency and high power THz generation.**
- (5) NP has successfully scaled the THz power to 0.339 mW by using the developed monolithic high power pulsed fiber lasers at ~ 1550 nm with longer nanosecond pulse width, and transform-limited narrow linewidth, based on a external cavity to enhance and recycle the fiber laser pumps.**
- (6) We have successfully demonstrated room temperature THz detection based-on THz upconversion by using the QPM-GaP crystal that will be used to develop the fiber-based high-resolution THz spectrometer in Phase II.**

In this project, NP Photonics proposes to implement and produce a fiber-based, compact, tunable, THz spectroscopic/fingerprinting system that offers ultra-high resolution (< 1 MHz), high sensitivity and room temperature operation over the 1-3 THz range. This proposed system provides high resolution molecular fingerprint information by leveraging NP Photonics high power and narrow linewidth fiber-based THz source, which is based on the newly developed THz crystal fiber converter and NP's high power single-frequency pulsed fiber lasers at eye-safe wavelength ~1550 nm in master oscillator and power amplifier (MOPA) configuration. Fig. 1 shows the schematic of the proposed compact, tunable, THz frequency source/detector system. Based on the successful demonstration in Phase I, in Phase II, the external cavity enhanced fiber-based THz source will generate 1-10 mW narrow linewidth THz radiation while providing for 3-4 decades of dynamic range. For the THz detection, we will implement a all fiber-based ultra-sensitive, room-temperature optical THz detection by using nonlinear parametric up-conversion based on our successful demonstration in Phase I. Terahertz radiation is mixed with pump light at ~1550 nm in the THz fiber converter to generate an optical sideband or idler wave that is coupled into optical fiber and detected using a Femtowatt Photoreceiver or GM-APD. The noise equivalent power (NEP) of this proposed THz detector is expected to be $\sim \text{fW/Hz}^{1/2}$ with a timing resolution of < ns.

NP Photonics uses our monolithic high power pulsed fiber laser system to achieve fiber laser pulses at ~ 1550 nm with high pulse energy, average and peak power, pulse width of > 500 ns, and transform-limited narrow linewidth ($< \text{MHz}$) for pumping the proposed ultra-high resolution THz source. The parametric THz generation is leveraged by a THz crystal fiber converter based on quasi-phase-matched (QPM)-GaP, which provides strong confinement of the two optical pumps and of the THz product, good overlap of the 3 optical fields over a long interaction length, and maintenance of the spatial synchrony between the induced polarization wave, and the electromagnetic wave product. In Phase II, NP Photonics will demonstrate the proposed THz source 1-10 mW power over the 1-3 THz range, and its footprint is smaller than $60 \times 60 \text{ cm}^2$ owing to the special compact advantages of fiber lasers. In the THz detection based on THz upconversion, optical detectors are a mature and commercial technology that offers excellent sensitivity with large bandwidths and room-temperature operation. As we demonstrated in Phase I in this project, InGaAs Femtowatt Photoreceiver or GM-APD enable detection down to the single photon limit with very fast performance. Therefore, this proposed fiber-based, compact, tunable, THz frequency source/detector system will have advantages of: (1) compact (footprint $< 60 \times 60 \text{ cm}^2$); (2) high spectral resolution ($< \text{MHz}$); (3) room temperature operation; (4) High temporal resolution ($< 1 \text{ ns}$); (5) high sensitivity ($\text{NEP} \sim \text{fW}/\text{Hz}^{1/2}$); (6) high stability for field applications; (7) safety (THz is safe for human body and fiber laser at ~ 1550 nm is eye-safe).

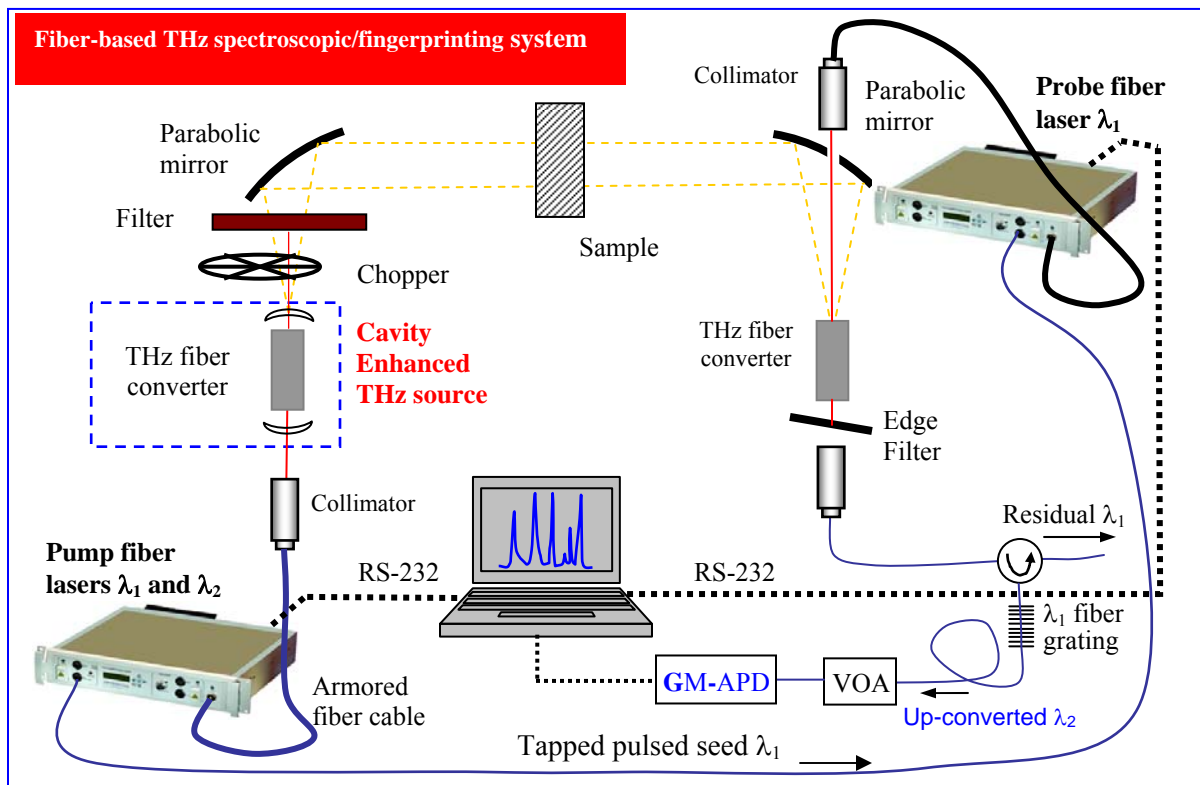


Fig. 1 Schematic of the proposed fiber-based, compact, tunable, THz spectroscopic/fingerprinting system with ultra-high resolution ($< 1 \text{ MHz}$), high sensitivity and room temperature operation.

2.0 PROJECT OBJECTIVES IN PHASE I

We have successfully carried out the following specific objectives in Phase I period:

- 1) Achieve monolithic high power fiber laser pulses with ~ 1 mJ pulse energy, average and peak power of 20W and 1-5 kW, pulse width of > 500 ns, and transform-limited narrow linewidth (< MHz) at ~ 1550 nm (eye-safe wavelength) based on NP's pulsed fiber laser seed and large core SM PM highly Er/Yb co-doped phosphate fibers.
- 2) Design and fabricate the optimized single mode THz crystal fibers as THz parametric converter by using the QPM-GaP structures under collaboration with Prof. Haus and Prof. Powers of UD.
- 3) Achieve mW-level ultra-narrow linewidth THz radiation based on single-pass DFG by using optimized single mode THz crystal fiber converter and monolithic high power fiber laser pulses.
- 4) Achieve ~ 10 mW ultra-narrow linewidth THz radiation based on our external cavity enhanced THz generation technique pumped by above high power pulsed fiber lasers by using THz crystal fiber converter with AR-coatings.
- 5) Demonstrate ultra-sensitive room-temperature THz detection based on THz parametric upconversion by using above high power pulsed fiber lasers and THz crystal fiber converter.
- 6) Demonstrate an ultra-narrow linewidth integrated high power THz array with 10-100 mW power over the 1-3 THz range, and its footprint is smaller than 60×60 cm² owing to the special compact advantages of fiber lasers. **(Optional and in Phase II)**
- 7) Design and build a fiber-based, compact, tunable, THz source/detector system that offers ultra-high resolution (< 1 MHz), high sensitivity and room temperature operation over the 1-3 THz range, which provides high-resolution molecular fingerprint information. **(Optional and in Phase II)**

3.0 WORK PERFORMED AND RESULTS OF PHASE I

3.1 All Fiber-Based THz Source

Table 1 summarizes the schemes for laser-based THz generation. One can see that among three kinds of compact THz sources, only fiber laser pumped parametric processes can not only generate high power narrow linewidth THz waves but also be operated without cryogen cooling at ambient temperature in the field. After we firstly demonstrated fiber-based THz source based on parametric processes, THz output power was scaled to 0.339 mW through scaling the average/peak power of Q-switched fiber lasers and increasing the conversion efficiency of the parametric processes. In Phase II of this project, the power of this narrow linewidth (< MHz) fiber-based THz source will be scaled to 1-10 mW for the proposed fiber-based, compact, tunable, THz frequency source/detector system shown in Fig.1.

Table 1. Summary of the schemes for laser-based THz generation.

SCHEMES	POWER	VOLUME	OPERATED TEMP.
Free Electron (THz) Laser	~ W	Very Bulky	Room-temp.
Optically pumped THz gas laser	~ 100 mW	Bulky	Room-temp.
Broadband THz pulses (Photoconduction & optical rectification)	~ μW	Bulky	Room-temp.
Current-injection laser (QCL)	~ mW	Compact	Cryogenic temp.
Fiber laser pumped photomixing	~ μW	Compact	Room-temp.
Fiber laser pumped parametric processes	~ mW	Compact	Room-temp.

(1) **Monolithic high power single-frequency pulsed fiber laser**

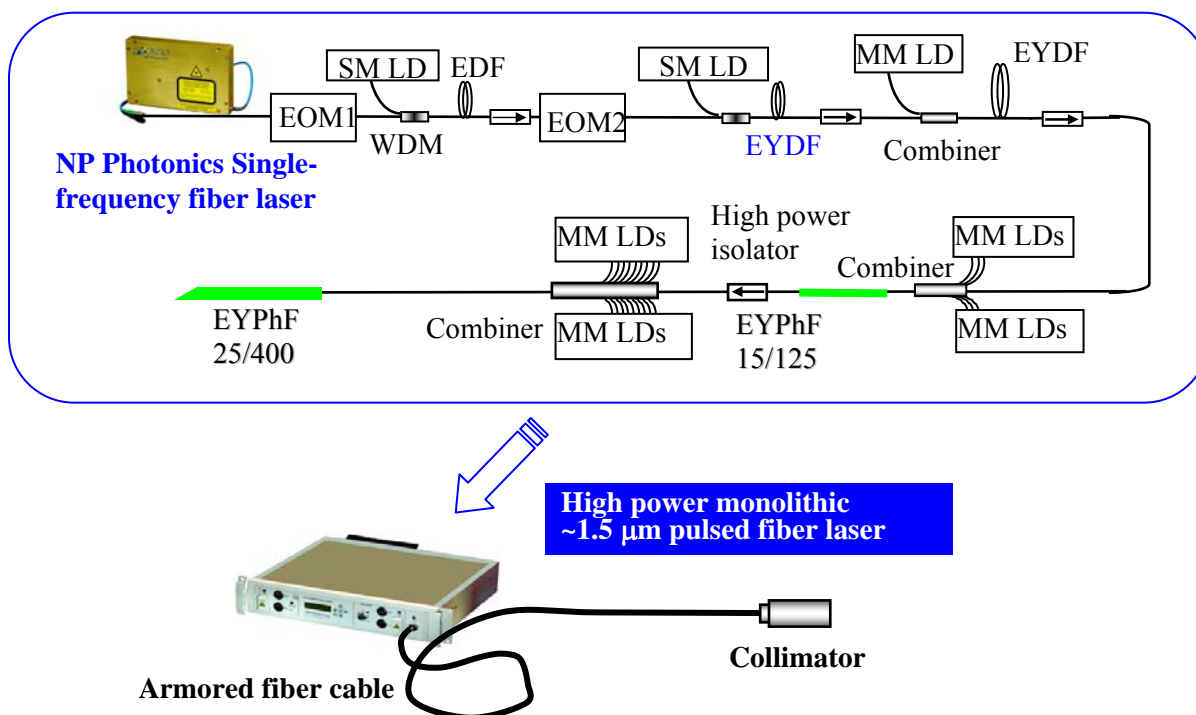


Fig. 2 Monolithic high power pulsed fiber laser system in MOPA.

Fig. 2 shows our current approach for high power single-frequency pulsed fiber laser, which we have developed in MOPA configuration based on NP’s newly developed SM PM highly Er/Yb co-doped phosphate fibers EYPhF 15/125, 25/400 and 30/250. Fig. 2 shows one of two implemented channels (1550.67 nm and 1538.74 nm) that were used for THz DFG. Their repetition rate can be tuned from tens of hertz to MHz. Most importantly, (1) the fiber laser pulsed seed is obtained by directly modulating the single-frequency fiber laser, which has the transform-limited narrow linewidth; (2) the pulse duration can be tuned from 2.5 ns to μ s controlled by an arbitrary waveform generator (AWG). In order to get the linewidth < MHz, we will use pulse width > 500 ns in this project. (3) Their wavelengths can be mode-hop-free tuned by piezo tuning of fiber laser, and thermally tuned in the range of \sim 30 GHz. Previously, we have demonstrated the highest peak power of \sim 128 kW when the repetition rate is 10 kHz and the pulse width 2-3 ns.

In this project, one of the core objectives is achieve the high peak power for the longer nanosecond (100ns- μ s) transform-limited fiber laser pulses by improving the stimulated Brillouin scattering (SBS)-threshold. In Phase I of this project, NP Photonics has successfully achieved significant progress for the longer nanosecond (100ns- μ s) transform-limited fiber laser pulses by leveraging on NP’s unique highly Er/Yb co-doped phosphate fibers with high unit gain for high SBS-threshold, in order to achieve the ultra-narrow linewidth fiber-based THz source for the proposed compact ultra-high resolution THz spectroscopic/fingerprinting system. In this project, NP Photonics proposed high resolution THz spectroscopic/fingerprinting system has the spectral resolution in < MHz level, and the linewidth and stability of the pulsed fiber laser should be less than < MHz.

because the fiber laser pulses are anticipated to have a transform-limited linewidth, the pulses duration must be large enough (~ 500 ns) in order to have a sufficiently narrow linewidth due to the transform-limit. For the sub-microsecond pulses with single spatial mode and very narrow linewidth, laser power scaling has been difficult in fiber amplifiers due to limitations primarily from the SBS nonlinear effect. SBS builds up strongly in the fiber for narrow linewidth pulses of long pulse duration. So it has been difficult to achieve high peak power, single-mode, and narrow linewidth operation simultaneously in a fiber laser system in a MOPA structure. Therefore, increasing the SBS threshold for the fiber amplifiers is crucial to scaling the peak/average power for the SM PM narrow linewidth sub-microsecond fiber laser pulses. There are three main approaches to reducing SBS effect or increasing SBS threshold. One is to reduce the overlap integral between the optical and acoustic field as accomplished by proper profile design. However, this approach is effective for passive fiber, not for LMA active fiber. The second is using a temperature gradient or strain gradient to alter the SBS spectrum along the fiber (which essentially shortens interaction length), but there is no high peak power narrow linewidth pulsed fiber laser reported yet using this approach. The last one that is the well-known approach to reduce the SBS effect is to make fibers with large mode area (LMA). The mode area is increased by lowering the core numerical aperture (NA) and increasing the core diameter. However, when the core diameter is larger than $20 \mu\text{m}$, the fiber becomes multimoded even with NA as low as 0.06. Modal discrimination, for example, induced by bending the fiber, can be used to achieve single mode operations. A side effect of this method is that for large core size, bending deforms the mode field distribution and thus reduces the mode area.

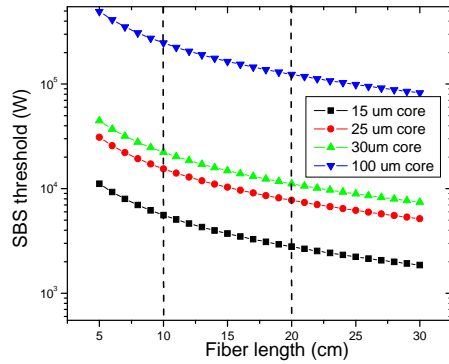


Fig. 3 Estimated SBS threshold vs. fiber length for 15/125, 25/400, 30/250, and 100/400 LC-EYPHF fibers.

In order to implement the high SBS-threshold amplifiers, we notice that the SBS threshold can be simply expressed as $P_{SBS} \sim 21 \frac{A_{eff}}{K \cdot g_B L_{eff}}$, where A_{eff} is optical effective mode area,

g_B the Brillouin gain coefficient $g_B = \frac{2m^7 p_{12}^2}{c\lambda^2 V_s \Delta v_{FWHM}}$, L_{eff} the effective length of the active fiber

($L_{eff} = \frac{1}{\exp(gL)} \int_0^L \exp(gz) dz$, where g is the unit gain of the active fiber), and K the polarization

dependence factor ($1/3 < K < 2/3$ when $L_{eff} \gg L_B$ where L_B is the polarization beating length). It is worth noting that our highly co-doping Er/Yb phosphate has the highest unit gain (> 5 dB/cm); resulting that the relative L_{eff} is smaller by one or two orders of magnitude compared to silica and silicate fibers. Furthermore, we have done the research about the SBS gain coefficient of our

phosphate fibers under collaboration with *Edward L. Ginzton Laboratory of Stanford University* recently. The results show that the SBS gain coefficient of our phosphate fibers is only half of that of a silica fiber.

According to the above analysis, in Fig. 3 we estimated the SBS threshold for our (large core) LC-EYPhF fibers with core size of 15 μm , 25 μm , 30 μm and 100 μm , respectively. One can see that when using 10-20 cm fiber length (as mentioned below, the optimized length for NP's LC-EYPhF in the range of 10-20 cm), the SBS threshold can be up to 2.8-5.6 kW for the 15 μm core phosphate fiber, 7.7-15 kW for 25 μm core fiber, 11.1-22.2 kW for 30 μm core fiber, and 123.8-247.5 kW for 100 μm core fiber, respectively. From these high estimated SBS-threshold in Fig. 3, it's is worth noting that NP's highly Er/Yb co-doped phosphate fiber has the highest possibility to achieve the highest peak power and pulse energy for SM PM sub-microsecond pulses with transform-limited pulse width. Actually, we have already achieved the highest peak power and pulse energy by using 15 μm , 25 μm and 30 μm core fibers, respectively, in Phase I.

15 μm core LC-EYPhF:

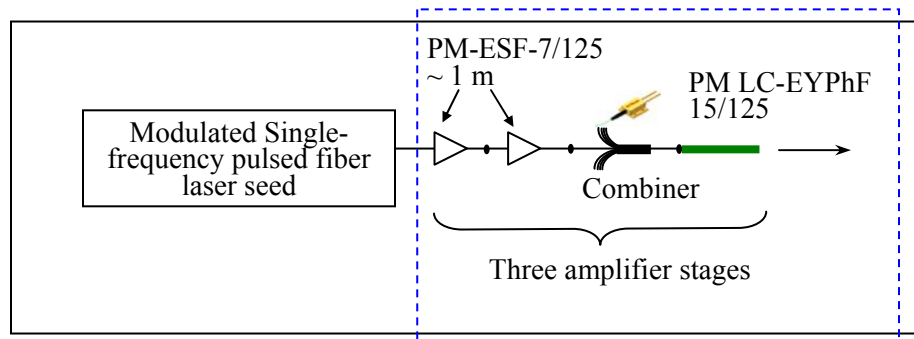


Fig. 4 Schematic of the SBS-free amplifier using NP fiber 15/125.

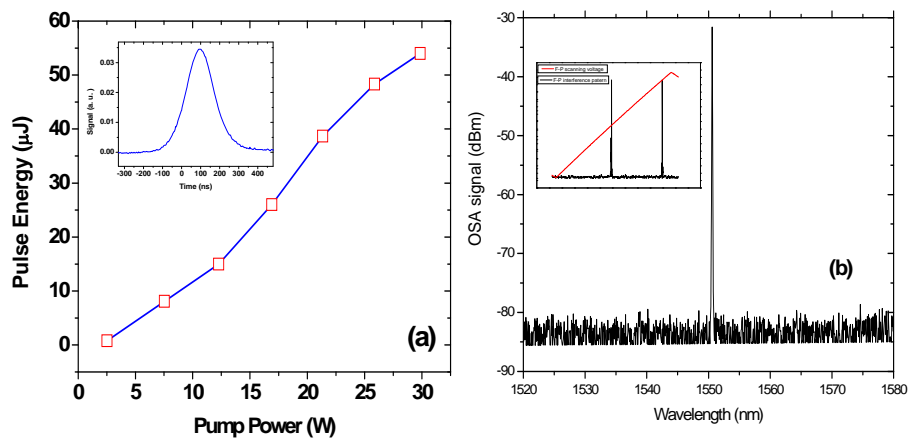


Fig. 5 (a) Pulse energies vs. pump power. (b) OSA spectrum and F-P scanning spectrum for the high-energy pulses at 1538 nm with repetition rate of 20 kHz.

Recently, we observed the SBS-free pulse energy of 54 μJ at 1538 nm with pulse duration of 153 ns based upon our large core SM PM LC-EYPhF 15/125 with 12 cm length shown in Fig.

4. This pulsed fiber laser system in MOPA is all fiber-based, no any free-space component included. The peak power is 352 W, transform-limited linewidth \sim MHz, and the beam quality $M^2 \sim 1.1$. This pulsed fiber laser system can be operated in the whole C-band. Fig. 5 (a) shows the typical performance of the MOPA system at ~ 1538 nm and the typical pulse shape (inset of Fig. 5 (a)). Fig. 5 (b) shows the OSA spectrum and Fabry-Perot (F-P) scanning spectrum (inset) of 54 μ J pulses. One can see that the in-band signal to noise ratio is nearly 50dB from the OSA spectrum. From the F-P scanning spectrum, it was estimated that the pulsed fiber laser in MOPA was operating in longitudinal single-mode and the transform-limited linewidth is about several MHz.

25 μ m core LC-EYPhF:

In Phase I of this program, we used the newly-developed SM PM highly Er/Yb co-doped phosphate fiber 25/400 with core size of 25 μ m to build the 2nd power amplifier stage of Fig. 6. By precisely controlling the indices of core and cladding glasses, the core NA of 25/400 fiber is as small as 0.0395, corresponding to a V number of $V = \frac{2\pi}{\lambda} aNA = 2.000 < 2.405$ that means this fiber is single mode fiber. In Phase I, we have optimized the fiber length of ~ 12 cm theoretically and experimentally.

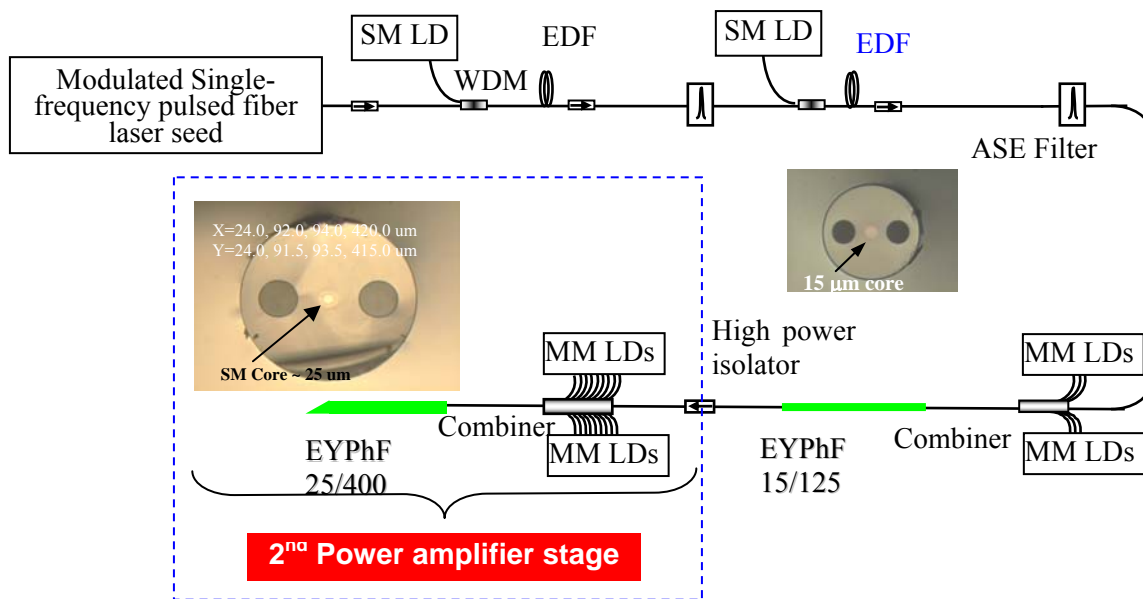


Fig. 6 Schematic of the 2nd power amplifier stage by using 25 μ m core fiber. Insert: cross section of the new large core highly Er/Yb co-doped phosphate fiber 25/400.

By using this newly developed SM PM large core highly co-doped phosphate fiber 25/400, the second power amplifier stage has been implemented. Fig. 6 shows the whole schematic of the monolithic pulsed fiber laser in MOPA, which have been designed and implemented for the high power/energy longer ns (> 100 ns) pulses with narrow linewidth. And one can see that the newly developed fiber has been successfully used in the final power amplifier stage with the optimized length of ~ 12 cm. NP Photonics phosphate-based gain fiber has the unique and dramatic feature of high gain per unit length. This makes possible high amplification in a short length and without SBS effect typical of conventional silica-based active

fibers. It is worth noting that the large core SM PM phosphate fiber has been successfully fusion-spliced with commercial silica fibers for the first time, which makes the whole MOPA system monolithic.

Fig. 7 (a) shows the output pulse energy at different pump powers for 112 ns pulse seed at 1530 nm with repetition rate of 8 kHz. One can see that the highest pulse energy can reach 0.126 mJ, which is the highest pulse energy for the longer ns pulses with transform-limited pulse width. Fig. 7 (b) shows the seed and amplified pulse shapes. One can see that the amplified pulse width 105 ns is a little narrower than the seed pulse width of 112 ns, and the amplified pulse shape is still Gaussian-like. Fig. 8 (a) shows the output peak power from the 2nd amplifier stage at different pump powers, which obtained by the pulse energy measurements in Fig. 7, pulse width, and repetition rate. It is worth noting that the highest peak power can reach 1.2 kW for 105 ns pulses with repetition rate of 8 kHz, which is the highest peak power for the longer ns pulses with transform-limited pulse width.

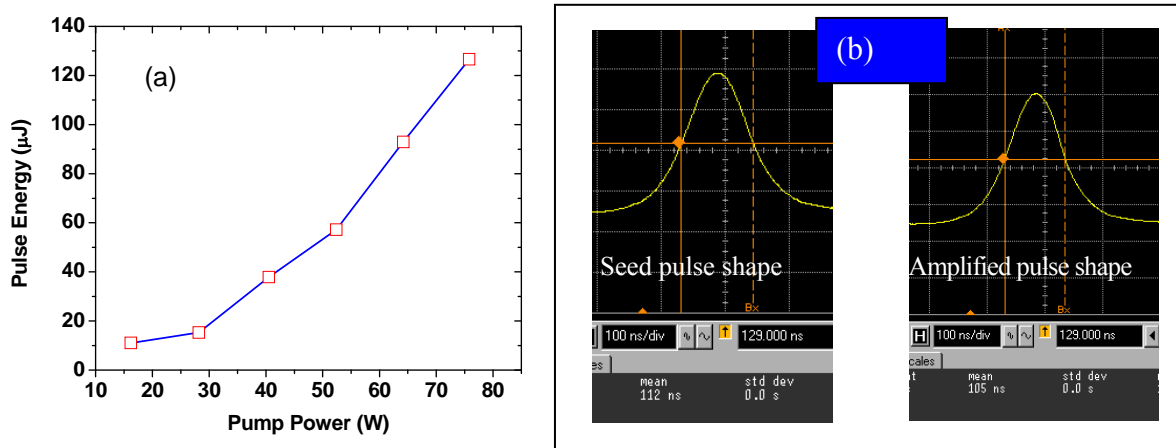


Fig. 7 (a) Output pulse energy of the 2nd amplifier at different pump power; (b) Pulse shape for the seed and amplified pulses.

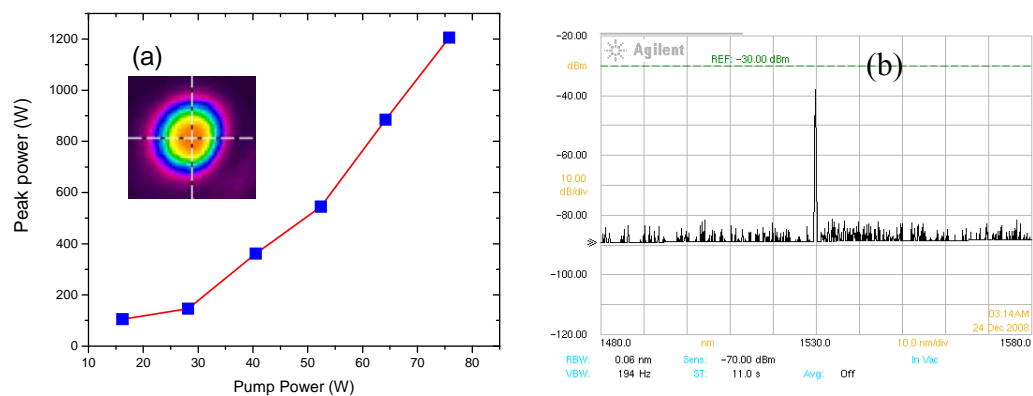


Fig. 8 (a) Output peak power of the 2nd amplifier at different pump powers; (b) Typical spectrum of the amplified pulses by the 2nd amplifier at 1530 nm.

The output beam quality of the fiber laser pulses with >100 μJ per pulse was characterized by a Spiricon Pyrocam III. Inset of Fig. 8 (a) shows the image of the pulsed fiber laser profile displayed in 2D view, which indicate the fiber laser pulses have diffraction limited

beam quality. The beam quality was also evaluated by measuring the M^2 values of around 1.2 for both vertical and horizontal directions through scanning the beam size around the waist position of the focused propagation beam. Fig. 8 (b) shows the spectrum of the amplified pulses when the peak power is about kW, which indicates the signal to noise ratio about 45 dB.

30 μm core LC-EYPhF:

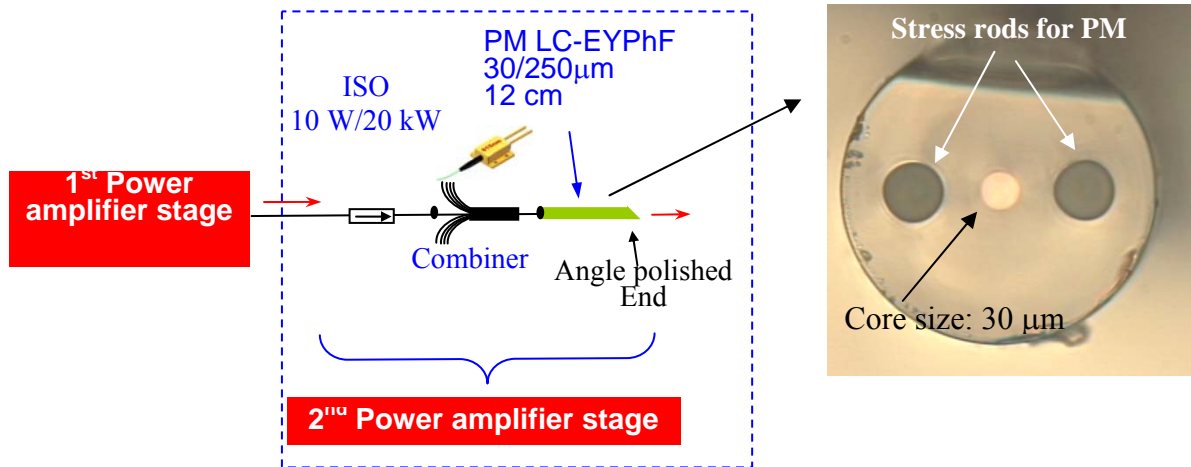


Fig. 9 Schematic of the 2nd power amplifier stage. Insert: cross section of the new large core highly Er/Yb co-doped phosphate fiber 30/250.

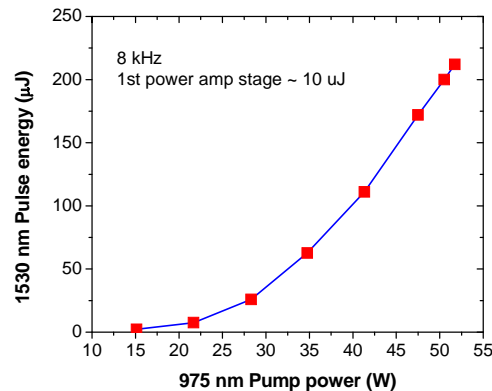


Fig. 10 SBS-free pulse energies vs. pump powers for the 2nd power amplifier stage by using 30/250 fiber.

In order to further increase the SBS threshold, NP Photonics has developed another new large core SM PM highly Er/Yb co-doped phosphate fiber 30/250 with core size of 30 μm . This new fiber has been designed and drawn in NP Photonics. Fig. 9 shows the fiber cross-section of the cleaved fiber end. One can see that this fiber is a PM fiber, and has a core size of 30 μm , which is the largest core size in the world for the phosphate active PM single-mode fiber. It is worth noting that the lowest core NA of 0.0395 has been achieved in NP Photonics by precisely controlling the index of the core /cladding glasses, which corresponds to a V number of $V = \frac{2\pi}{\lambda} aNA = 2.400 < 2.405$ that means this fiber is single mode fiber.

By using this fiber in the 2nd power amplifier stage, the transform-limited pulse energy has been successfully improved in Phase I of this project. Fig. 10 shows the pulse energy at 1530 nm with SBS-free when using different pump level for the 2nd power amplifier stage. The final

pulse width is about 100 ns and repetition rate 8 kHz. One can see that the maximum SBS-free pulse energy can be up to 0.212 mJ, which corresponds to a peak power of 2.12 kW, average power of 1.696 W and conversion efficiency of 3.28%. This pulse energy is the highest fiber-based pulse energy for the longer pulses (> 100 ns) with transform-limited linewidth.

100 μ m core Leakage Channel Fiber with Single-mode Performance:

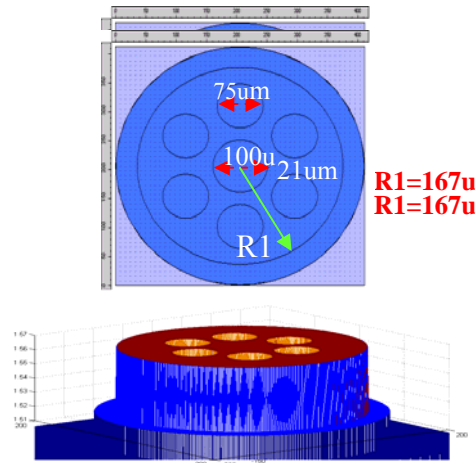


Fig. 11 Design of the new all-glass leakage channel fiber.

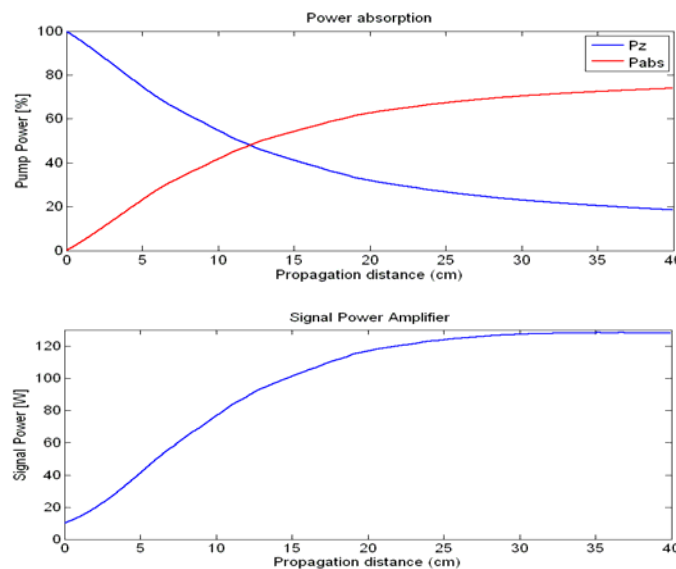


Fig. 12 Simulation of the power performance for the designed LCF to be used as amplifier fiber with 40 cm length.

In Phase II of this project, NP Photonics will demonstrate mJ-level SBS-free transform-limited fiber laser pulses with 100-500 ns pulse width, corresponding to ~ 100 kW peak power. In order to significantly improve the SBS threshold and achieve the highest peak power for efficient narrow linewidth THz generation, in Phase II, we will design and fabricate the first SM PM large core highly Er/Yb co-doped phosphate leakage channel fiber (LCF) with core size of ~ 100 μ m. The preliminary structure design of 100 μ m core photonic crystal fiber is shown in Fig. 11. One can see the SM performance is formed by leakage channel design. The polarization maintaining

of leakage channel fiber is introduced by the stress rods shown in Fig. 11. Based on our calculation, the fiber core should be close to 100 μm , even by using NP's high unit gain phosphate fiber. Fig. 12 shows the power performance simulation results for the designed LCF (in Fig. 11) to be used as amplifier fiber with 40 cm length, when using 10 W seed and 450W pump power. One can see that the highest output power can reach ~ 120 W. Especially, the expected SBS-threshold can be up to ~ 100 kW.

(2) **Narrow linewidth of the fiber-based THz source**

In this project, the narrow linewidth of the fiber-based THz source is critical for the proposed ultra-high resolution (< 1 MHz) and high sensitivity molecular THz fingerprint system. Firstly, NP's fiber-based THz source has very fine tunability. From Fig. 2, one can see our pulsed fiber laser start from NP Photonics single-frequency fiber lasers. The piezo tuning range of the fiber laser is 200 MHz with a tuning rate of ~ 10 MHz per voltage applied to the piezo. So, the tuning step can be down to $< \text{kHz}$ -level. The thermal tuning range 30 GHz with a tuning rate 1 GHz/ $^{\circ}\text{C}$. The proposed THz source is based on the difference-frequency generation of two fiber laser pumps, so the proposed THz source has the same frequency tuning range and tuning rate. The wide range tuning from 0.2 to 6 THz can be easily achieved by changing the NP Photonics fiber laser seed with different center wavelength. The aforementioned tunability is very crucial for high resolution molecular fingerprint information. Secondly, NP's fiber-based THz source can reach very high spectral resolution. From Fig. 2, one can see that our pulsed fiber laser pumps are operated by directly chopping the single-frequency fiber laser, therefore the linewidth is transform-limited. The electrical pulses used to drive two EOMs are generated from an AWG card, which can have programmable waveform and any pulse width above ~ 500 ns. Therefore, in this project, in order to achieve the narrow linewidth ($< \text{MHz}$) optical pulses, we have successfully controlled the pulse spectral linewidth by using longer pulse widths based on NP's proprietary unique fiber laser pulse seed in Phase I. The linewidth of THz source depends on the pump linewidth for the DFG process. Thirdly, the average power of the fiber-based THz source should be higher enough. In Phase I of this project, we have successfully scaled the THz power to 0.339 mW by using the developed monolithic high power pulsed fiber lasers at ~ 1550 nm with longer nanosecond pulse width, and transform-limited narrow linewidth, based on a external cavity to enhance and recycle the fiber laser pumps.

3.2 **THz Crystal Fiber Converter for High Power Parametric THz source**

In pursuing the high power THz generation based on optical parametric processes, previously, the PI has successfully used several bulk THz crystals, such as GaSe, ZnGeP₂, GaP, to achieve the high power THz parametric generation. Recently, we noticed that the QPM-GaP and GaAs materials have been developed and the larger samples are available currently. However, the generated THz peak power is still below the results obtained by using bulk crystals. Initially, the main reason is that the length of QPM samples is limited due to the trade-off between the length and interface loss. However, the high quality QPM crystals did not produce high power either. The most important reason is the poor overlap of the three interaction beams due to THz divergence in the optical parametric processes and the small optical beam size ($< 100\text{s } \mu\text{m}$) for the THz wavelength, when using bulk crystal or QPM materials. Considering the THz divergence, the THz conversion efficiency should be modified as:

$$\eta' = \frac{1}{2} \left(\frac{\mu_0}{\epsilon_0} \right)^{3/2} \frac{\omega_1^2 d_{\text{eff}}^2 L^2}{n_1 n_2 n_3} \left(\frac{P_3}{A} \right) T_1 T_2 T_3 \exp(-\alpha_1 L) \left(\frac{1 - \exp(-\Delta\alpha L / 2)}{\Delta\alpha L / 2} \right)^2 \times \left(\frac{A_{\text{THz}}}{A_{\text{Optical}}} \cdot \Gamma^2 \right) \quad (1)$$

where $\left(\frac{A_{\text{THz}}}{A_{\text{Optical}}} \cdot \Gamma^2 \right)$ is the modified factor, Γ the overlap factor between the normalized power distribution of the optical beam and the normalized electric field distribution of the THz waves. In order to increase the modified factor, several approaches have been reported, such as rod-type waveguide, polymer cladding silicon core waveguide, and integrated GaAs optical waveguide. None of these approaches resolves the problem very well. From Eq. (1), in order to achieve the highest THz conversion efficiency and highest parametric THz generation, the following factors should be considered simultaneously: (1) phase-matching, (2) high effective nonlinear coefficient, (3) nonlinear interaction length, (4) low absorption of THz materials at pump and THz ranges, (5) high pump power (peak power), (6) beam size and overlap factor between the optical pump beams and the THz waves. Therefore, NP Photonics proposes a single mode THz crystal fiber as THz parametric converter, by using QPM-GaP materials, in order to achieve the highest parametric THz conversion efficiency and highest THz power. In Phase I of this project, NP Photonics has successfully demonstrated this new structure—the single mode THz crystal fiber as THz parametric converter, including the development of the QPM GaP materials (see Fig. 13). This is the first demonstration of the single mode THz crystal fiber converter.

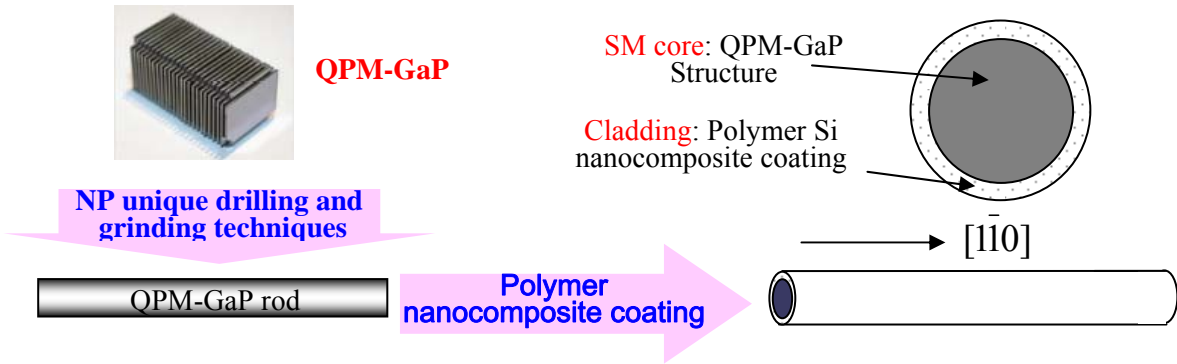


Fig. 13 Schematic of the fabrication for the single mode THz crystal fiber converter.

(1) QPM-GaP crystals

Previously, tunable THz DFG was achieved in bulk GaP with $\sim 1 \mu\text{m}$ pump sources and THz tuning range can be from 0.106-4.22 THz. GaP crystal has zinc blende structure with symmetry group of F43m, so its linear optical properties are isotropic and it has no birefringence. For THz generation based on optical parametric processes in GaP pumped by near infrared lasers, phase-matching conditions can still be achieved because THz wavelengths pass through reststrahl region. Theoretically, exact collinear phase-matched DFG for THz generation can only be obtained when pump wavelengths are in the range from 0.995 to 1.033 μm for bulk GaP crystal. However, it's still difficult to achieve the high power THz radiation by using these pump wavelengths due to multi-photon absorption with a GaP band gap of about 2.26 eV. In addition, we are still short of high quality laser sources in the wavelength range of 0.995 μm -1.033 μm for parametric processes. In order to achieve high power THz generation, in this experiment we use bonded QPM-GaP crystals with different numbers of periods pumped by high power pulsed fiber lasers in the C-band. In addition GaP has no two-photon absorption at our pump wavelength ($\sim 1.5 \mu\text{m}$), and a second order nonlinear coefficient $\chi^{(2)}$ ($d_{14} \sim 30\text{pm/V}$) close to that of LiNbO₃ (d_{33}

$\sim 34.4\text{pm/V}$). In order to best use nonlinearity of GaP, (110) undoped GaP wafers were used for preparing the QPM structures and have high resistivity $\sim 10\text{ M}\Omega\text{-m}$ with carrier concentration $\sim 10^9\text{ cm}^{-3}$. Fig. 14 (a) shows the orientation of these GaP wafers. The calculated coherence length is $551.5\text{ }\mu\text{m}$ based on GaP index dispersion, when using 1550 nm and 1538 nm pulsed fiber laser pumps to generate difference frequency of 1.5 THz . Fig. 14 (b) shows the pictures of the bonded QPM-GaP crystals with different layer numbers of coherence length. The measured THz absorption coefficient is about 1.6 cm^{-1} at 1.5 THz for the bonded QPM-GaP crystals.

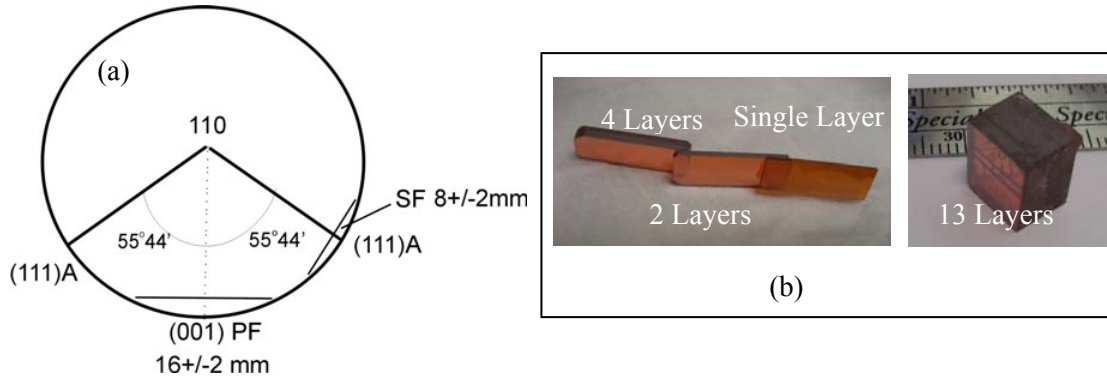


Fig. 14 (a) Orientation of the GaP wafers for QPM-GaP structures; (b) Pictures of the bonded QPM-GaP crystals.

(2) **Single-pass THz generation using QPM-GaP crystals**

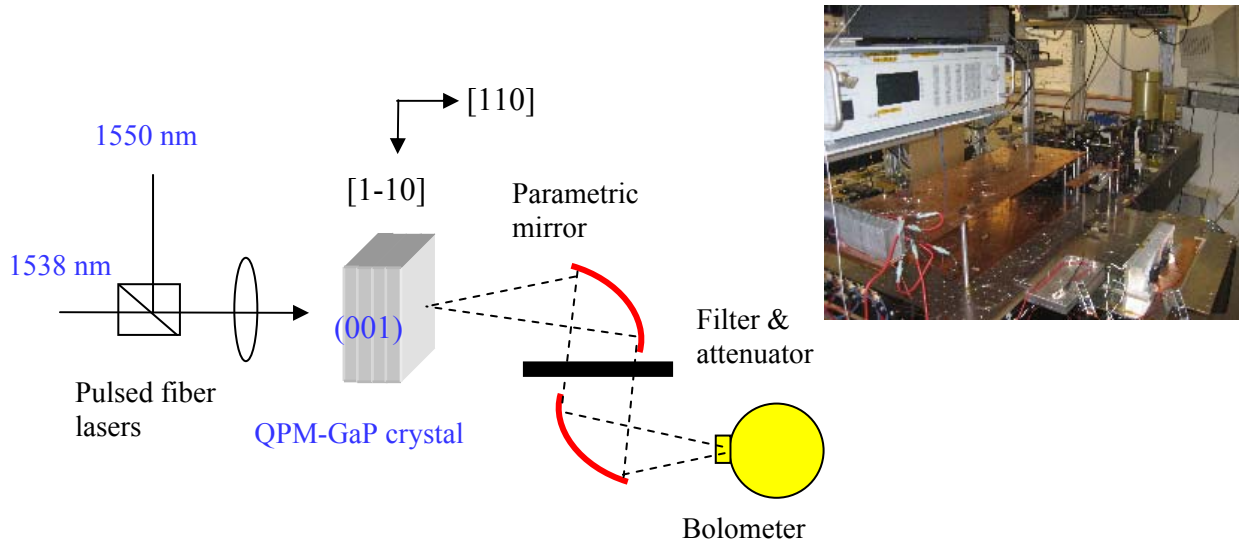


Fig. 15 Schematic and picture of the setup for single-pass THz generation by using QPM-GaP crystals.

The two pulsed fiber lasers in MOPA configuration that are realized by directly modulating two single-frequency fiber lasers (1550nm and 1538nm) were used to pump the QPM-GaP crystals for single-pass THz generation, based on DFG. The generated THz signal was measured by using a calibrated bolometer. Two temporally overlapped pulses ($\sim 80\text{ns}$, 20 kHz) from two fiber lasers in MOPA configuration are combined using a polarizing beam splitter, and then focused into QPM-GaP crystal for the single-pass THz generation by using the experimental setup shown in Fig. 15.

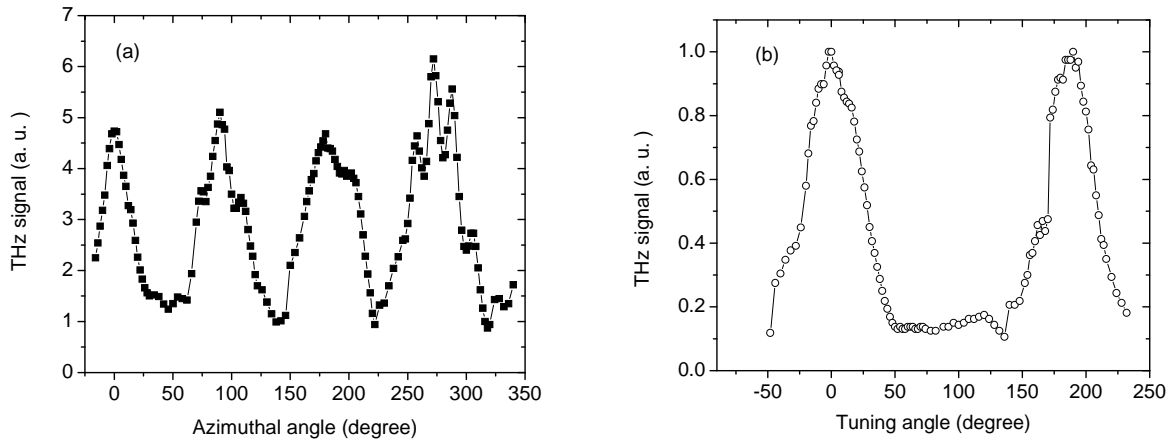


Fig. 16 THz generation for GaP-QPM structures when the polarization directions of two pump beams are (a) orthogonal and (b) parallel.

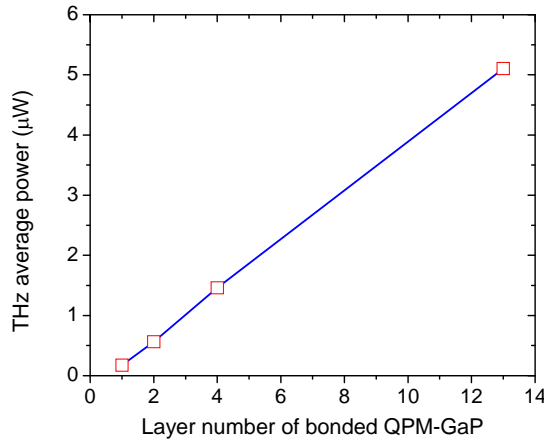


Fig. 17 Single-pass DFG THz average powers for different bonded QPM-GaP crystals.

In order to optimize the effective second-order coefficients for the QPM-GaP crystals in experiments, the azimuthal dependence of the THz generation in (110) plan for the GaP QPM bonded structures has been measured when the polarization directions of two pump beams are orthogonal and parallel, respectively. Fig. 16 shows the THz generation for the GaP QPM bonding structures when the polarization directions are orthogonal and parallel. For orthogonal polarization direction in Fig 16 (a), one can see that the generated THz signal reaches the maximum values when the one of the pump polarizations is along the [001] direction. For the parallel polarization direction in Fig. 16 (b), the generated THz signal reaches the maximum value when the pump polarizations are along the [111] direction. Fig. 17 shows the single-pass DFG THz average powers for different bonded QPM-GaP crystals when using orthogonal polarization directions and one of the pump polarization is along the [001] direction. The pump pulse energy we used is about 53.3 μJ for two pulsed fiber laser pumps. One can see that the generated THz average power for 13-layer bonded QPM-GaP is about 5.1 μW, which is 29 times higher than that for single layer GaP with coherence length, and corresponds to a conversion efficiency of 4.78×10^{-6} .

(3) Optimization of the coherence length by using a GaP wedge

For the above QPM-GaP crystals, we used the theoretical THz indices to calculate the coherence length for the GaP crystals. The coherence length of 551.5 μm was determined by using GaP index dispersion, when using 1550 nm and 1538 nm pulsed fiber laser pumps to generate difference frequency of 1.5 THz. In order to achieve the optimized QPM-GaP structures, we demonstrated the optimization of coherence length of GaP in experiments by using a polished GaP wedge crystal, for the first time.

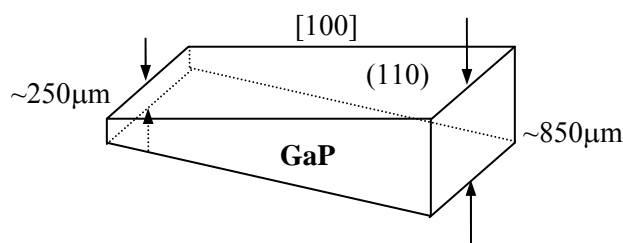


Fig. 18 Polished wedge sample using the high purity (110) GaP wafer.

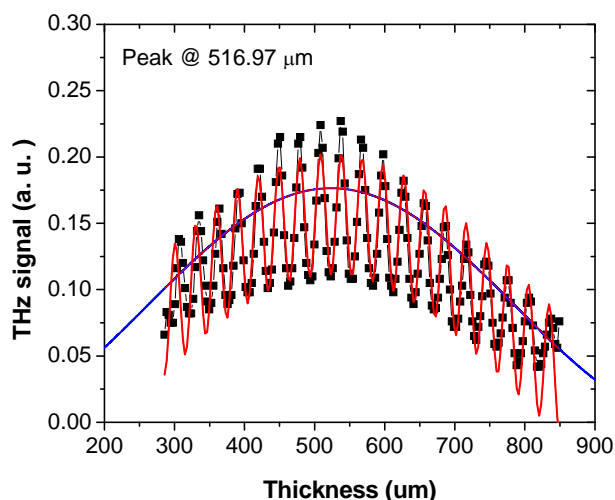


Fig. 19 THz generation at different thickness for the wedge sample.

In order to best use GaP's second order nonlinearity for THz generation, we choose the high purity GaP wafers that have relatively low absorption in THz range. A 2-inch GaP wafer with thickness of ~ 1 mm was used to make a wedge sample shown in Fig. 18. Its orientation is shown in Fig. 14 (a). One can see the thickness of the wedge sample is from ~ 250 μm to ~ 850 μm , and two (110) facets were polished. Then the THz generation was detected at different thicknesses for the wedge sample shown in Fig. 19. NP's 1550 nm and 1538 nm pulsed fiber laser pumps (orthogonally polarized to each other) were used to generate difference frequency of 1.5 THz. In Fig. 19, the symbols indicate the measured THz radiation values at different thickness, the red curve represents the fitting of the experimental data, and the blue curve shows the fitted profile of the experimental results. From Fig. 19, one can see that the measured results show a very well-defined interference pattern when changing the wedge thickness. From the fitted profile curve, we can clearly see the generated THz signal increases then decreases when the thickness of wedge changes from ~ 250 μm to ~ 850 μm . Therefore, the coherence length of 516.97 μm

corresponds to the thickness when THz signal reaches the maximum, which is different by 34.53 μm compared with the calculated coherence length. From this measured coherence length, we can determine the THz index 3.33675 at 1.5 THz based on near-IR indices of GaP and momentum mismatching defined as $|\Delta k| = |k_3 - k_2 - k_1|$, where k_3 , k_2 , and k_1 correspond to the wave vectors for the THz wave and two pump beams. The theoretical value of THz index at 1.5 THz is 3.32464. On the other hand, we can verify the THz wavelength by using the interference pattern in Fig. 19 and the measured THz index of GaP: $\lambda = 2n_T d_{p-p} = 198\mu\text{m}$, where d_{p-p} is the distance between two adjacent peaks in the interference pattern.

(4) THz waveguide modeling for high efficiency and high power THz generation

In Phase I, the UD team worked on several modeling efforts to help THz guide device designs for boosting THz performance. Finally, we will this design to fabricate the THz waveguide nonlinear crystal (or THz waveguide crystal converter) in NP Photonics, in order to achieve the high efficiency and high power THz generation.

The first set of models look at THz generation using difference frequency generation (DFG) in a waveguide. The UD team put together two waveguide models; one assumes cylindrical symmetry (and hence runs fast) while the second allows an arbitrary two-dimensional waveguide structure such as a ridge-waveguide. A second modeling effort focused on ‘‘photon recycling’’ has also been initiated. In the DFG process, two inputs (pump and signal) are incident at the input to the crystal waveguide, which then generate the THz difference frequency. In this process, the THz is generated, the pump is depleted, and the signal is amplified. In the DFG process, most of the energy goes to the signal photon, and the photon recycling idea looks at using this excess energy to further amplify the THz signal. Both modeling efforts are described below.

Waveguide models

Modeling the DFG process centers on the wave equation, which is derived in several textbooks. We do not reproduce the derivation here, but go straight to the working equations and then highlight the salient features. For the DFG process in a waveguide, three coupled amplitude equations are given by,

$$\frac{dA_1}{dz} = \frac{i}{2k_{1,\text{core}}} \nabla_{\perp}^2 A_1 - \frac{\alpha_1(x,y)}{2} A_1 - i \frac{(n_{1,\text{core}}^2 - n_1(x,y)^2)}{2k_{1,\text{core}}} \frac{\omega_1^2}{c^2} A_1 + i \frac{\omega_1^2}{k_{1,\text{core}} c^2} d_{\text{eff}} A_2 A_3 e^{-i\Delta k z} \quad (2)$$

$$\frac{dA_2}{dz} = \frac{i}{2k_{2,\text{core}}} \nabla_{\perp}^2 A_2 - \frac{\alpha_2(x,y)}{2} A_2 - i \frac{(n_{2,\text{core}}^2 - n_2(x,y)^2)}{2k_{2,\text{core}}} \frac{\omega_2^2}{c^2} A_2 + i \frac{\omega_2^2}{k_{2,\text{core}} c^2} d_{\text{eff}} A_1 A_3^* e^{i\Delta k z} \quad (3)$$

$$\frac{dA_3}{dz} = \frac{i}{2k_{3,\text{core}}} \nabla_{\perp}^2 A_3 - \frac{\alpha_3(x,y)}{2} A_3 - i \frac{(n_{3,\text{core}}^2 - n_3(x,y)^2)}{2k_{3,\text{core}}} \frac{\omega_3^2}{c^2} A_3 + i \frac{\omega_3^2}{k_{3,\text{core}} c^2} d_{\text{eff}} A_1 A_2^* e^{i\Delta k z} \quad (4)$$

where A is the field amplitude, α is the linear absorption coefficient, n_{core} is the index of refraction in the core of the waveguide, $n(x,y)$ is the index as a function of transverse direction (in the core $n_{\text{core}}^2 - n(x,y)^2 = 0$), ω is the angular frequency of the field, k is the wavevector magnitude, d_{eff} is the nonlinearity, and Δk is given by $k_1 - k_2 - k_3$. Each equation shows terms that account for diffraction, loss, waveguiding, and nonlinear coupling. Solving for output fields is accomplished by using a split-step approach, which has had great success in modeling three-wave interactions. The temporal profile of the fields is assumed to be slowly varying so that we may segment up a pulse into several pieces, solve for each segment separately, and then at the end add up the contributions from each segment. Such a procedure works well for narrow

bandwidth pulses and is appropriate for nsec and longer pulse durations. Reducing the computation time for the models is greatly increased by assuming cylindrical symmetry, as might be expected in a nonlinear fiber. We do not go into the details here, but the main difference between cylindrical symmetry and no symmetry is in how we work with the transverse Laplacian. With cylindrical symmetry we use a 1-dimensional Hankel transform whereas with no symmetry we use a 2-dimensional Fourier transform. In our initial work, we benchmarked the two models against each other and found that they both give the same results when the waveguide structure exhibits cylindrical symmetry. As seen in Equations (2) through (4) there are a many variables that enter into the equations, each of which may depend on wavelength. Our models incorporate all of the variables separately to give us the greatest flexibility. The cylindrically symmetric model's front panel is shown in Fig. 20. We developed a similar front-panel for modeling a ridge waveguide, which is shown in Fig. 21.

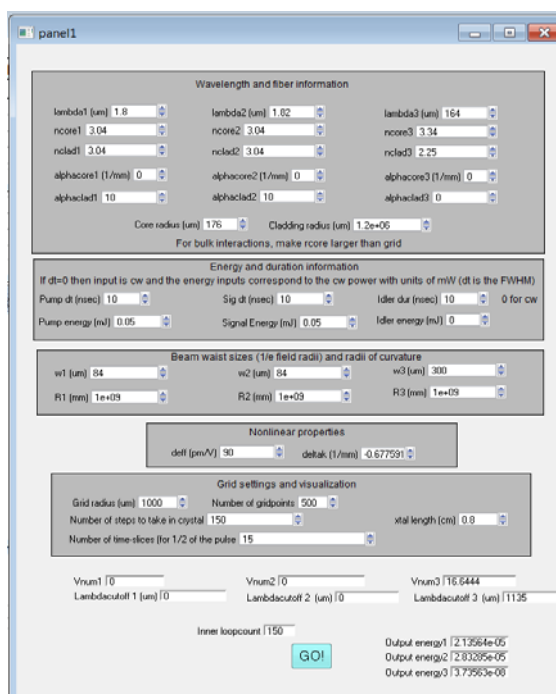


Fig. 20 Front panel for cylindrically symmetric waveguide designs. This front panel lets us quickly change variables and see how they affect the performance of the device.

Both models are operational, however most of our current efforts in working with the models has centered on the cylindrically symmetric one. In the next quarter we will start comparing the ridge waveguide designs to the cylindrically symmetric designs. Currently, we have looked at optimizing the waveguide structures for THz generation. The first set of simulations looked at the effects of the core diameter and the size of the input beams. Fig. 22 shows a plot of THz output as a function of the core radius and as a function of input beam radius (Gaussian). Fig. 22 a) shows a continuous wave simulation and Fig. 22 b) shows a 10 nsec pulse simulation. The input powers for Fig. 22 a) were 100W in both the inputs and for b) the input energies were 50 μ J in each input. The cladding material is a nanocomposite material, which has an index of 2.25 at the THz. The cladding material is assumed to scatter the inputs, which we model by increasing the absorption of the two inputs in the cladding layer. For each point in the figure, Δk was optimized for peak performance.

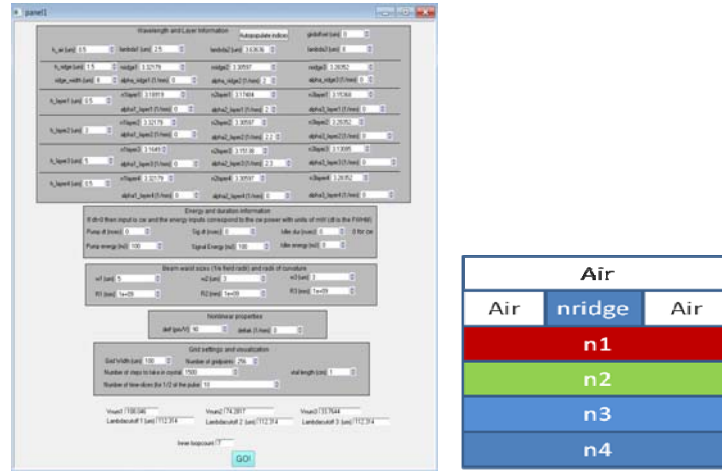


Fig. 21 a) Front panel for modeling nonlinear interactions in a ridge waveguide structure. b) Waveguide structure. Note that we control the indices and the layer thicknesses from the front panel.

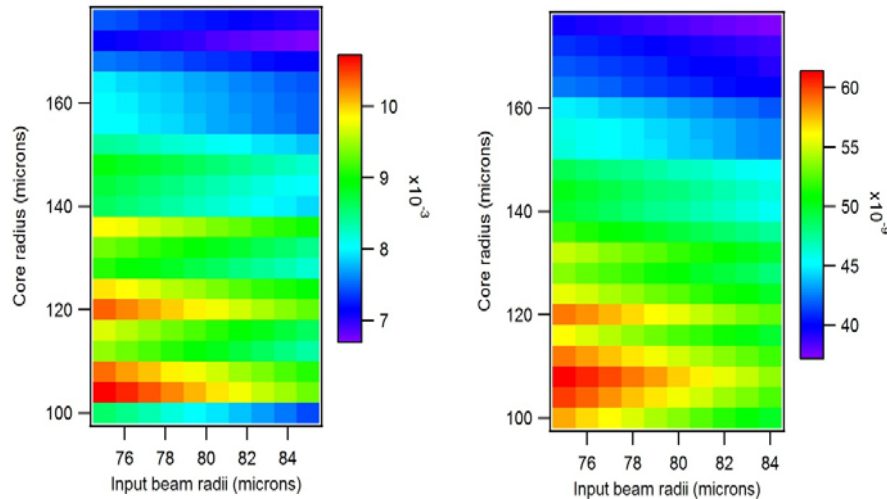


Fig. 22 a) THz power as a function of input beam radius and waveguide core radius (power is in W). The input powers were 100W each. b) THz pulse output energy as a function of input beam radius and waveguide core radius (energy is in J). The input pulse energies were 50 μ J in 10 nsec pulses (FWHM). Both simulations used a 1 cm interaction length.

Fig. 22 shows that in general, it is advantageous to focus the inputs as tightly as possible. Other simulations over a broader range of input beam radii show the same trend. However, crystal damage limits how tightly one may focus. The monotonic increase in power of energy with decreasing beam size is attributed to the fact that the near-IR inputs do not diffract significantly over the 1 cm interaction length. We chose the range Fig. 22 so as to focus more on the effects of the core radius on the performance. Fig. 23 shows the dependence on core radius when the input beam size is 75 μ m. The figure shows an optimum core radius in the neighborhood of 115 μ m. The oscillations are attributed to interference effects that occur due to the core-cladding interface. Note that such effects are present in the waveguide because of the relatively short interaction length. Being able to see such features is a strength of this numerical

approach, it does not rely on describing the interaction in terms of waveguide modes, rather it simply propagates the fields in the structure.

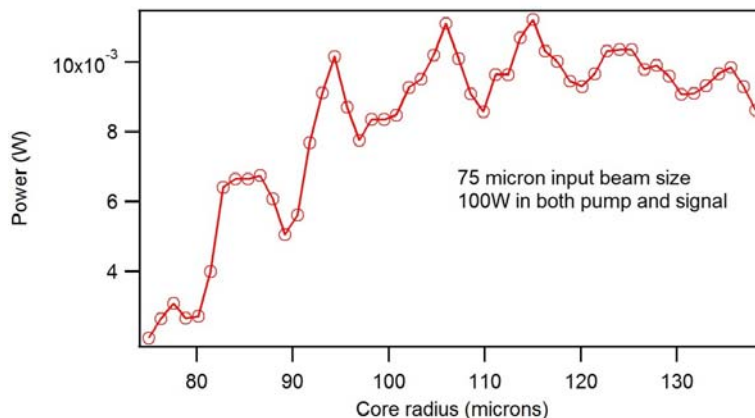


Fig. 23 A closer look at core size on THz output power. The line is included to guide the eye.

In Phase II, under collaboration with Prof. Joseph W. Haus and Peter E. Powers from Nonlinear Optics Lab & the Electro-Optics Program of University of Dayton (UD), we will further investigate and design the guided parametric THz generation, and develop and optimize the proposed THz crystal fiber converters. Also, NP Photonics will further optimize the drilling process in order to fabricate the uniform rods and protect the end surfaces, in order to fabricate the optimize THz crystal fiber converter for high power ultra-resolution THz source.

3.3 Fiber-Based High Spectral Resolution THz Spectrometer

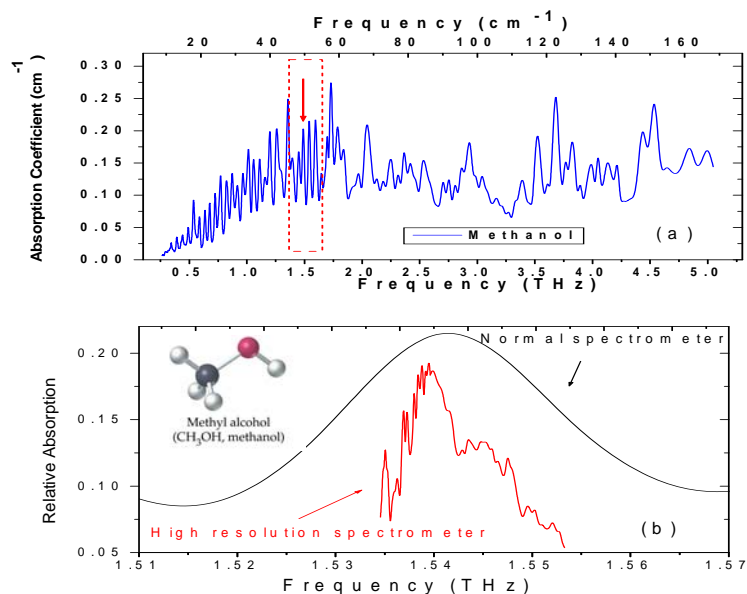


Fig. 24 Characterization of the resonant peaks of methanol vapor: (a) measured by previous THz spectrometer; (b) measured by using the high resolution THz spectrometer based on the NP's new narrow linewidth THz source.

PI has implemented a tabletop high spectral resolution spectrometer by using NP's narrow linewidth THz source. The resonant peaks of methanol vapor (CH_3OH) have been distinguished by

using such a high spectral resolution spectrometer. Fig. 24 (a) shows the resonant peak structures as determined by using the THz source with \sim GHz-level linewidth (Wei Shi et al, "Fingerprinting molecules based on direct measurement of spectrum by frequency-tuning monochromatic THz source," *Laser physics letters*, Vol. 1, No.: 11, 560-564 (2004)). Fig. 24 (b) shows the resonant peak structures by using the high resolution THz spectrometer based on NP's new narrow linewidth THz source. From Fig. 24, it's worth noting that the high resolution THz spectrometer can distinguish <10 s MHz-FWHM resonant peak. On the other hand, this high resolution THz spectrometer conforms that linewidth of NP's high power THz source can be narrower than 1 MHz, which depends on the transform-limited of the pulse width. In this project, we will demonstrate the ultra-narrow linewidth ($<$ MHz) THz source and ultra-high resolution THz spectrometer by using \sim 500 ns fiber laser pulses based on Fig. 2's MOPA system.

3.4 External Cavity Enhanced THz Generation

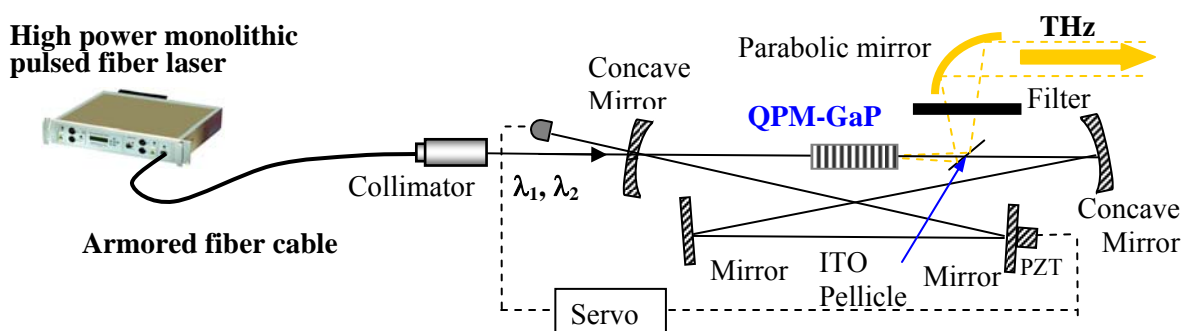


Fig. 25 Schematic of the cavity enhanced THz source.

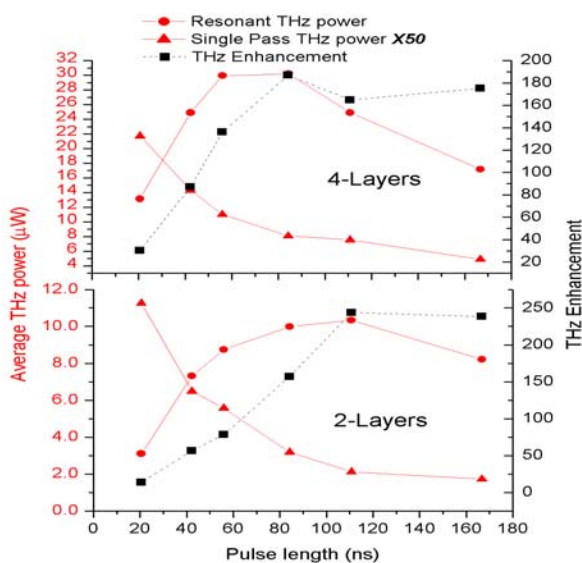


Fig. 26 Cavity enhanced and single-pass THz power (multiplied by 50), and cavity enhancement factor for two and four layers of QPM-GaP crystals when using the fixed fiber laser pulse energy of 18.3 μ J and different pulse widths.

Recently, NP Photonics has successfully demonstrated a new method to produce single frequency THz radiation by enhancing and recycling nanosecond fiber laser pulses in an external ring cavity with an intracavity ZGP, for the first time. In Phase I of this project, we

demonstrated a large increase in cavity enhancement and average output THz power using QPM GaP. To achieve a large cavity enhancement for two separate input beams a simple cavity is vital to reduce aligning complexity. The previously used crystal (ZGP) is birefringent and to phase-match at $\sim 1.5 \mu\text{m}$ perpendicular polarizations are needed, which creates a walk off of the two orthogonal pump beams. This necessitated using intracavity edge filters to separately align each wavelength, increasing complexity and cavity losses. By employing QPM-GaP in the external cavity; the cavity and cavity alignment has been significantly simplified. The optical cavity is arranged in a bow tie shape as seen in Fig. 25 with total length $\sim 0.65 \text{ m}$. It is stabilized by a third (1550 nm) CW laser traveling in the opposite direction around the cavity then picked off by an edge filter to avoid destabilizing fluctuations in the locking signal from the nanosecond pulses. The QPM-GaP crystal is located at the waist between two concave mirrors with radius of curvature 0.25 m. Two input couplers $M1$ (17%, 8%) were used to impedance match the cavity loss depending on which crystal was used (2 and 4 layers QPM-GaP crystals). The cavity is pumped by two temporally overlapped pulsed fiber lasers in MOPA configuration at 20 KHz. They are combined in a polarizing beam splitter and mode matched to the cavity.

For a given intracavity QPM crystal there is a trade-off between the number of periodic layers and the losses they incur inside the cavity in order to achieve highest THz average power. In addition, for an optical cavity and associated losses there is an optimum pulse width that optimizes input peak power for efficient THz DFG and resonant pulse enhancement where they scale as inverse and proportional respectively to the pulse width. Thus we chose to test this by measuring THz enhancement for different pulse widths with 2 and 4 layers of QPM-GaP crystals shown in Fig. 14. The different width pulses (20 ns-170 ns) all had pulse energy of $18.3 \mu\text{J}$ geometric mean of the two laser channels and similar pulse shapes. We can see a peak in the overall THz average power at $\sim 110\text{ns}$ for the 2-layer sample and $\sim 80\text{ns}$ for the 4-layers. The difference in pulse width to achieve peak power is due to higher losses in the 4-layer sample leading to lower pulse enhancement, which favors shorter pulse lengths with higher peak power. Fig. 26 also includes the cavity enhancement factors and single-pass THz output powers when using the fixed fiber laser pulse energy of $18.3 \mu\text{J}$ and different pulse width. One can see that the cavity enhancement factor increases when the pulse width increases. For 2-layer and 4-layer QPM-GaP crystals, the cavity enhancement factors can be up to ~ 250 and ~ 190 when the pulse width increases to $\sim 110 \text{ ns}$ and $\sim 80 \text{ ns}$, respectively. For the single-pass cases, the generated THz power decreases when the pulse width increases due to the pump peak power decreasing. It is possible that more QPM layers will result in a higher cavity enhanced THz power due to the longer QPM interaction length but we were limited to the samples at hand. We did test the 13-layer GaP sample for the cavity enhanced THz DFG but found the transmission loss too high to get more efficient cavity enhancement, as demonstrated, the cavity enhancement factor is very sensitive to the cavity loss.

We then chose to use the optimum pulse width 80 ns for 4-layer QPM-crystal in order to achieve higher cavity enhanced THz output power by using higher pulse energy for the pulsed fiber laser pumps in Fig. 25. Fig. 27 shows the average THz powers for cavity enhanced single-pass cases when using different pulse energy up to $70 \mu\text{J}$ with pulse width of 80 ns. We can see that both the single pass and resonantly enhanced data follow a quadratic curve as would be expected in a second order nonlinear interaction. From a quadratic fit of the data we can see an enhancement of 151 times over the single pass case. The maximum external cavity enhanced THz average power can reach $339 \mu\text{W}$ and peak power $\sim 212 \text{ mW}$ when the pump pulse energy is

about 70 μJ . This maximum THz output power corresponds to a THz power conversion efficiency of 2.43×10^{-4} and quantum efficiency of 3.16%. The pulsed fiber laser pumps are transform-limited, and the expected linewidth is about 10 MHz. Due to the parametric process (DFG), the generated THz waves are expected to have the same narrow linewidth level. So, the spectral power density for the generated THz signal can be up to ~ 33.9 W/THz.

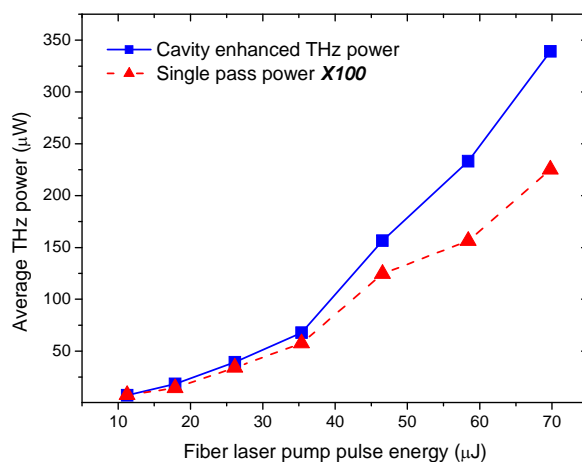


Fig. 27 Cavity enhanced and single pass THz power vs. pump pulse energy when using pulse width 80 ns at 20 kHz repetition rate.

3.5 Ultra-Sensitive Room-Temperature THz Detection Based-on THz Upconversion

(1) THz upconversion detection

In order to achieve ultra-high resolution (< 1 MHz), high sensitivity and room temperature molecular fingerprint measurements, an ultra-sensitive, fast and room temperature THz detector is critical. However, compared to the near infrared, terahertz technology is relatively immature. For the THz detection, room-temperature direct detectors like Golay cells and pyroelectric have poor sensitivities. Other commercial THz detectors, like bolometers, are much more sensitive but require liquid helium cooling and like their room-temperature counterparts have small electrical bandwidths. In order to pursue the efficient and coherent THz detection at room-temperature, the PI has successfully used several bulk THz crystals, such as GaSe, ZnGeP₂ (ZGP), GaP, to achieve the THz parametric detection based on the THz upconversion. Fig. 28 shows the setup for the detection of THz up-converted signal. Fig. 29 shows PI measured THz upconverted results based on THz parametric upconversion by using GaSe and ZGP. Recently, we noticed that the QPM-GaP materials have been developed and the larger samples are available currently. In Phase I, NP has successfully achieved high power high efficient THz generation by using QPM-GaP structure pumped by using NP's high power pulsed fiber lasers. Most importantly, we have observed the THz up-converted signal based on Fig. 28's setup, for the first time. In Phase II of this project, we will use QPM-GaP structure as THz upconverter to detect the THz waves based on Fig. 30's all fiber-based setup, in order to demonstrate the fiber-based high-resolution THz spectrometer. In Phase II, NP Photonics will demonstrate the proposed all fiber-based, compact, tunable, THz spectroscopic/fingerprinting

system (see Fig. 1) that offers ultra-high resolution (< 1 MHz), high sensitivity and room temperature operation over the 1-3 THz range.

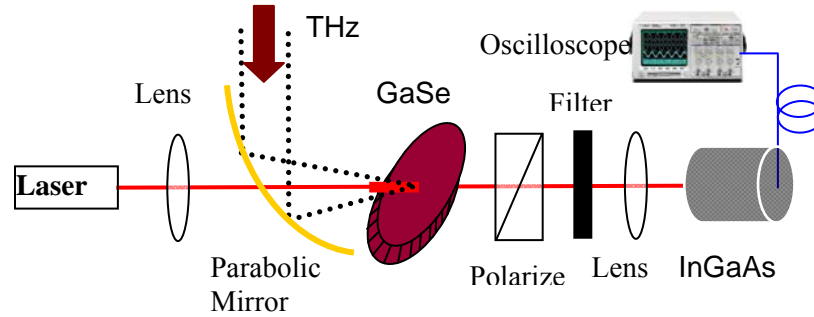


Fig. 28 Schematic of up-converted THz detection.

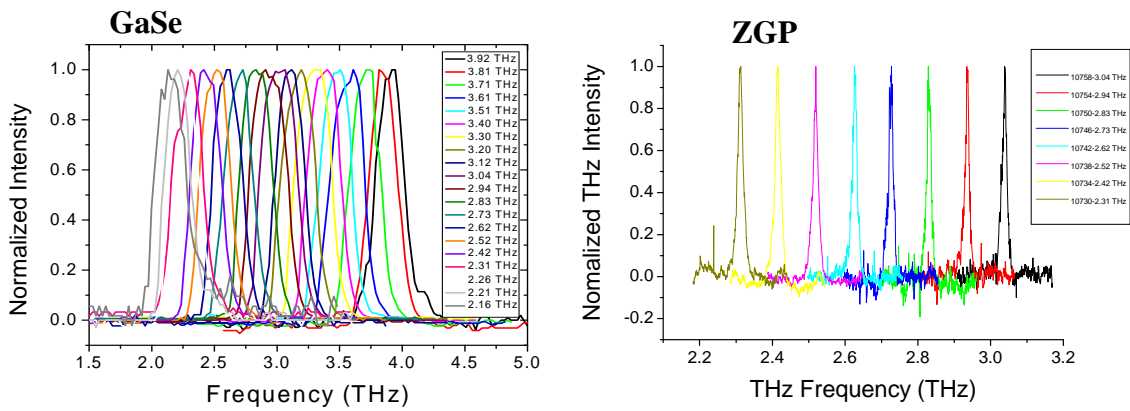


Fig. 29 Measured THz spectrum results based on parametric THz upconversion.

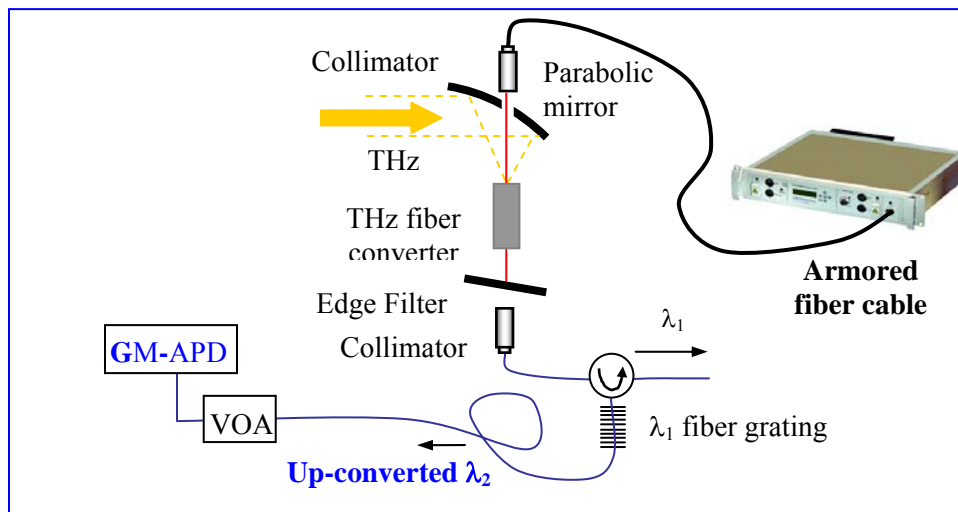


Fig. 30 Fiber-based THz detector based on THz parametric upconversion.

4.0 ESTIMATIONS OF THE TECHNICAL FEASIBILITY AND CONCLUSIONS

4.1 Achievements in Phase I

In Phase I, NP Photonics has successfully demonstrated the feasibility to implement the proposed fiber-based, compact, tunable, THz spectroscopic/fingerprinting system. The pulse energy of NP pulsed fiber lasers with transform-limited linewidth have been scaled up to 0.212 mJ, which corresponds to a peak power of 2.12 kW by using the new developed NP single-mode PM large core fiber 30/250. This pulse energy is the highest fiber-based pulse energy for the longer pulses (> 100 ns) with transform-limited linewidth. We have achieved the bonded QPM-GaP crystals and the proposed THz crystal fiber converter for high power parametric THz source. We have optimized coherence length for GaP crystal by using a GaP wedge, and demonstrated a new approach to verify the THz wavelength by using the GaP wedge. THz waveguide modeling has been developed for high efficiency and high power THz generation In Phase I by the UD team, which can be used for the design to fabricate the THz waveguide nonlinear crystal (or THz waveguide crystal converter) in NP Photonics, in order to achieve the high efficiency and high power THz generation. NP has successfully scaled the THz power to 0.339 mW by using the developed monolithic high power pulsed fiber lasers at ~ 1550 nm with longer nanosecond pulse width, and transform-limited narrow linewidth, based on an external cavity to enhance and recycle the fiber laser pumps. We have successfully demonstrated room temperature THz detection based-on THz upconversion by using the QPM-GaP crystal that will be used to develop the fiber-based high-resolution THz spectrometer in Phase II.

4.2 Core Objectives in Phase II

Based on the achievements and successful demonstration in Phase I, NP Photonics proposes to carry out the following specific objectives during Phase II period:

- (1) In order to significantly improve the SBS threshold and achieve the highest peak power for efficient narrow linewidth THz generation, in Phase II, we will design and fabricate the first SM PM large core highly Er/Yb co-doped phosphate leakage channel fiber (LCF) with core size ~ 100 μm and cladding size ~ 400 μm .
- (2) Achieve monolithic high power fiber laser pulses with ~ 1 mJ pulse energy, average and peak power of 20W and 1-5 kW, pulse width of > 500 ns, and transform-limited narrow linewidth ($< \text{MHz}$) at ~ 1550 nm (eye-safe wavelength) based on NP's pulsed fiber laser seed and large core SM PM highly Er/Yb co-doped phosphate LCF fiber 100/400.
- (3) Further design and fabricate the optimized QPM-GaP structures and single mode THz crystal fibers as THz parametric converter by using the QPM-GaP structures under collaboration with Prof. Haus and Prof. Powers of UD about the fundamental design.
- (4) Demonstrate ultra-narrow linewidth THz radiation based on single-pass DFG by using optimized QPM-GaP crystals, single mode THz crystal fiber converter and monolithic high power fiber laser pulses.
- (5) Achieve 1-10 mW ultra-narrow linewidth THz radiation based on our external cavity enhanced THz generation technique pumped by above high power pulsed fiber lasers by using QP-GaP crystals and THz crystal fiber converter with AR-coatings.
- (6) Demonstrate ultra-sensitive room-temperature THz detection based on THz parametric upconversion by using above high power pulsed fiber lasers, QPM-GaP crystals and THz crystal fiber converter.

- (7) Demonstrate an ultra-narrow linewidth integrated high power THz prototype with 1-10 mW power over the 1-3 THz range, and its footprint is smaller than $60 \times 60 \text{ cm}^2$ owing to the special compact advantages of fiber lasers.
- (8) Design and build a table-top fiber-based, compact, tunable, THz source/detector system that offers ultra-high resolution ($< 1 \text{ MHz}$), high sensitivity and room temperature operation over the 1-3 THz range, which provides high-resolution molecular fingerprint information.
- (9) Measure and investigate the THz spectroscopy of low-pressure molecular vapor by using the proposed high-resolution THz spectrometer under cooperation with Prof. Haus and Prof. Powers of University of Dayton about the fundamental THz spectroscopic research.

4.3 Commercial applications of the Innovation

The proposed fiber-based ultra-high resolution THz spectroscopic/fingerprinting system can be of immediate use as a standalone product as its anticipated unique features and capabilities are not available now on the market. In addition to the detection of molecular fingerprint information, it will be a promising THz source/detector for homeland security, especially for the remote sensing and imaging of hazardous materials, such as drugs and poison chemicals due to its high power, tunable high frequency and high resolution, as well as for nondestructive evaluation (NDE). This THz spectroscopic/fingerprinting benefits from the unique narrow linewidth, tunability and high stability of our fiber-based THz source, so this THz sensor will have very high resolution, very high sensitivity, and very low noise. The proposed new approaches in both THz generation and detection will improve the current investigations in THz spectroscopy, sensing and imaging, and detection and identification of molecular fingerprint information and hazardous materials for homeland security. Three prototypes will be developed in Phase II: 1) ultra-narrow linewidth integrated high power fiber laser; 2) ultra-narrow linewidth compact high power fiber-based THz source; 3) proposed fiber-based ultra-high resolution THz spectroscopic/fingerprinting system. These three prototypes will be further developed and commercialized as NP' final products in Phase III.

5.0 REFERENCES

- (1) **Wei Shi***, E. Petersen, N. Moor, A. Chavez-Pirson, N. Peyghambarian, All fiber-based single-frequency Q-switched laser pulses at 2 μm for LIDAR and remote sensing applications, *SPIE Nano-and Macrophotonics for Space Environments Conference V-2011, San Diego, California, 21-25 August 2011 (Invited Talk)*
- (2) Eliot Petersen, **Wei Shi***, Arturo Chavez-Pirson and Nasser Peyghambarian, Efficient parametric terahertz generation in quasi-phase-matched GaP through cavity enhanced difference-frequency generation, *Applied Physics Letters*, Vol. 98, No. 13, 121119 (2011)
- (3) **Wei Shi***, E. Petersen, Arturo Chavez-Pirson and N. Peyghambarian, Coherent monolithic THz generation based on quasi-phase-matched GaP bonding structures pumped by pulsed fiber lasers at $\sim 1.5 \mu\text{m}$, *SPIE Photonics West 2011, LASE-Nonlinear Optics, San Francisco, California, 23 - 27 January 2011*
- (4) **Wei Shi***, Eliot Petersen, Dan T. Nguyen, Zhidong Yao, Jie Zong, Mark A. Stephen, Arturo Chavez-Pirson and Nasser Peyghambarian, "Kilowatt-level SBS-threshold monolithic transform-limited 100 ns pulsed fiber laser at 1530 nm," *Optics Letters*, Vol. 35, No. 14, 2418-2420 (2010).
- (5) **Wei Shi***, E. Petersen, Arturo Pirson, N. Peyghambarian, "Fiber-based THz sources based on high power single-frequency pulsed fiber lasers at 1.55 μm ," SPIE Photonics West 2010, LASE-Nonlinear Optics, San Francisco, California, 23 - 28 Jan., 2010 (**Invited talk**)
- (6) **Wei Shi***, M. A. Leigh, J. Zong, Z. Yao, A. Chavez-Pirson and N. Peyghambarian, "High power all fiber-based narrow linewidth single-mode fiber laser pulses in the C-band and frequency conversion to THz generation," *IEEE J SEL TOP QUANT* **15**, 377-384 (2009)
- (7) **Wei Shi***, Eliot B. Petersen, Matthew Leigh, Jie Zong, Zhidong Yao, Arturo Chavez-Pirson, and Nasser Peyghambarian, "High SBS-threshold single-mode single-frequency monolithic pulsed fiber laser in the C-band," *Opt. Express* **17**, 8237-8245 (2009)
- (8) **Wei Shi***, Matthew Leigh, Jie Zong, Zhidong Yao, and Shibin Jiang, "Photonic Narrow Linewidth GHz Source Based on Highly Codoped Phosphate Glass Fiber Lasers in a Single MOPA Chain," *IEEE Photonics Technology Letters*, Vol. 20, No. 2, Jan. 15, 69-71 (2008).
- (9) **Wei Shi***, Matthew Leigh, Jie Zong, Shibin Jiang, "Single-frequency THz source pumped by Q-switched fiber lasers based on difference-frequency generation in GaSe crystal," *Optics Letters*, Vol. 32, No. 8, 949-951 (2007)
- (10) **Wei Shi** and Yujie J. Ding, "Tunable coherent radiation from terahertz to microwave by mixing two infrared frequencies in a 47-mm-long GaSe crystal," *International Journal of High Speed Electronics & Systems*, Vol. 16, No. 2, 589-604 (2006)
- (11) **Wei Shi** and Yujie J. Ding, Nils Fernelius and F. Ken Hopkins, "Observation of difference-frequency generation by mixing of terahertz and near-infrared laser beams in a GaSe crystal," *Applied Physics Letters*, Vol. 88, 101101 (2006)
- (12) **Wei Shi** and Yujie J. Ding, "Generation of backward terahertz waves in GaSe crystal," *Optics Letters*, Vol. 30, No. 14, 1861-1863 (2005)
- (13) **Wei Shi** and Yujie J. Ding, "Tunable terahertz waves generated by mixing two copropagating infrared beams in GaP," *Optics Letters*, Vol. 30, No.9, 1030-1032 (2005)
- (14) **Wei Shi** and Yujie J. Ding, "Fingerprinting molecules based on direct measurement of spectrum by frequency-tuning monochromatic THz source," *Laser physics letters*, Vol. 1, No.: 11, 560-564 (2004)
- (15) **Wei Shi** and Yujie J. Ding, "A monochromatic and high-power THz source tunable in the ranges of 2.7–38.4 μm and 58.2-3540 μm for variety of potential applications," *Applied Physics Letters*, Vol. 84, No. 10, 1635-1637 (2004).
- (16) **Wei Shi**, Yujie J. Ding, and P. G. Schunemann, "Coherent terahertz waves based on difference-frequency generation in an annealed zinc-germanium phosphide crystal: improvements on tuning ranges and peak powers," *Optics Communications*, Vol. 233, No. 1-3, 183-189 (2004)
- (17) **Wei Shi**, Yujie J. Ding, "Designs of THz waveguides for efficient parametric THz generation," *Applied Physics Letters*, Vol. 82, No. 25, 4435-4437 (2003)
- (18) **Wei Shi**, Yujie Ding, Changshui Fang, Qiwei Pan, Qingtian Gu, "Investigation of charge effects on poling and stability for corona-poled polymer films," *Applied Physics A: Materials Science & Processing*, Vol. 77, No. 3-4, 567-570 (2003)
- (19) **Wei Shi**, Yujie J. Ding, "Continuously tunable and coherent terahertz radiation by means of phase-matched difference-frequency generation in zinc germanium phosphide" *Applied Physics Letters*, Vol. 83, No. 5, 848-850 (2003)
- (20) **Wei Shi**, Yujie J. Ding, "Coherent and widely tunable THz and millimeter waves based on different-frequency generation in GaSe and ZnGeP₂," (Optics in 2002), *Optics & Photonics News (OPN)*, Vol. 13, No. 12, 57 (2002)
- (21) **Wei Shi**, Yujie J. Ding, Nils Fernelius, Konstantin Vodopyanov, "Efficient, tunable, and coherent 0.18-5.27 THz source based on GaSe crystal," *Optics Letters*, Vol. 27, No. 16, 1454-1456 (2002)